



Supplementary Materials for

Reconstitution of an intact clock reveals mechanisms of circadian timekeeping

Archana G. Chavan *et al.*

Corresponding authors: Carrie L. Partch, cpartch@ucsc.edu; Andy LiWang, aliwang@ucmerced.edu

Science **374**, eabd4453 (2021)
DOI: 10.1126/science.abd4453

The PDF file includes:

Materials and Methods
Figs. S1 to S22
Tables S1 to S12
References

Other Supplementary Material for this manuscript includes the following:

MDAR Reproducibility Checklist
Data S1 to S8

Materials and Methods

Cloning, expression and purification of proteins:

PCR-mediated mutagenesis was performed on the pET-28b vector utilizing Nde I/Hind III restriction sites as described previously (58) to modify clock genes from *Synechococcus elongatus* to produce 6x-His-SUMO fusion proteins in *Escherichia coli* BL21(DE3) (Agilent). All constructs are listed in **Table S1**. Point mutations were introduced using long-range PCR with overlapping primers (14). A single colony from freshly transformed cells was used for inoculation of a starter culture grown in LB medium supplemented with 50 µg/mL kanamycin sulphate at 37 °C, 220 rpm. After 6.5 h a 5 mL starter culture was transferred to 1 L M9 medium supplemented with 0.2% D-glucose, 2 mM MgSO₄, 0.1 mM CaCl₂, and 50 µg/mL kanamycin sulfate. Cells were grown to OD₆₀₀ ≈ 0.6 at 37 °C before inducing expression by addition of 0.2 mM isopropyl β-d-1-thiogalactopyranoside (IPTG) and incubating cells at 30 °C for 12 h, except for CikA expression for which cells were incubated at 20 °C for 22 h.

Cells were harvested and lysed using an Avestin C3 Emulsiflex homogenizer (Avestin Inc, Canada). Cell lysate was clarified by high-speed centrifugation before affinity purification on Ni-NTA resin (QIAGEN) in polypropylene gravity columns using the buffers specified in Table S1. All purification steps were carried out at 4 °C. For cleavage of the 6x-His-SUMO fusion protein, 6x-His-ULP1 protease was added to final concentration of 3 µM and incubated at 4 °C for 15 h. Reductant tris(2-carboxyethyl)-phosphine (TCEP) was added to SasA and CikA samples during ULP1 cleavage (concentrations given in **Table S2**). 6x-His-SUMO was removed by loading the cleaved protein on a Ni-NTA column for a second time. The flow-through was concentrated using 10 kDa molecular weight cut-off (MWCO) membrane filters in an AmiconTM (Millipore Sigma) stir-celled concentrator at 4 °C before purifying by gel-filtration chromatography. SasA used for two-dimensional titration experiments was purified as His-Gβ1-tagged full-length SasA constructs over Ni-NTA resin using the standard protocol described previously (14), followed by overnight cleavage at 4°C with TEV protease with final concentration of 0.1 mg/mL. SasA was subsequently resolved from the His-Gβ1 tag on a Sephadex 200 size-exclusion column (GE Healthcare) equilibrated with 20 mM Tris, 150 mM NaCl pH 7.4.

Fluorescent labeling of proteins:

N-terminal sortase-mediated ligations were performed for full-length protein constructs used in IVC that had been modified to carry an N-terminal glycyl residue (see **Table S3**). The fluorophore-containing peptides 5-carboxyfluorescein (5-FAM)-LPETGG and C-(Cy3)-LPETGG were purchased from GenScript (New Jersey). For C-terminal ligations, target proteins were fused to sortase-A recognition peptide LPETGG at the C-terminus. The peptide GGGYCN was expressed and purified in-house as a 6x-His-SUMO-fusion protein. The cysteinyl residue on the purified fusion protein was labeled with the fluorophore 6-iodoacetamidofluorescein (6-IAF) (Invitrogen) as described previously (25). The labeled peptide was cut from the SUMO-fusion protein using ULP1 and passed through 10 kDa MWCO membrane in stirred cell concentrator. The flow-through containing labeled peptide was further purified by C4 reverse-phase column chromatography. The peptide was eluted with a linear acetonitrile gradient and then lyophilized. Dried peptide was dissolved in sortase buffer before use. Concentration was determined by UV absorbance by the 6-IAF fluorophore at 493 nm. Each target protein was buffer exchanged in sortase buffer (20 mM Tris, 150 mM NaCl, pH 7.5) before ligation. For ligation, 50 μ M target protein was incubated with 250 μ M fluorophore peptide, 5 μ M sortase-A, and 10 mM CaCl_2 in the dark at 4 °C for 12-16 h. Sortase-A was separated from reaction mixtures by Ni-NTA chromatography using prepacked 5 mL HiTrap-Ni-NTA columns (GE Healthcare) on an AKTA FPLC using a step gradient of imidazole. Labeled protein fractions were concentrated and purified further by gel-filtration chromatography using a Superose-6-Increase-10/300 GL analytical grade column (GE Healthcare). Table S2 lists the fluorophore peptides used for labeling each protein construct. Fluorescence labeling of fsKaiB, SasA_{trx}, and CikA_{psr} constructs was done with 6-iodoacetamidofluorescein (6-IAF, Invitrogen) as described previously (37).

Reconstitution of clock reactions for fluorescence anisotropy measurements:

For monitoring multiple probes simultaneously, a master mix of oscillator reactions was prepared in 20 mM Tris, 150 mM NaCl, 5 mM MgCl_2 , 1 mM ATP, and pH 8.0 buffer by mixing unlabeled proteins at the final concentrations shown in **Table S4**, except for KaiC and fluorescently labeled probes. IVC reactions were initiated by adding a solution of KaiC and ATP to the master mix. Aliquots (95 μ L) of reaction master mix were pipetted into black, non-binding

384-well microplates (Greiner BioOne). Finally, 5- μ L aliquots of fluorophore-labeled protein (50 nM final concentration) or DNA (100 nM final concentration) were added to separate wells. The plate was sealed using clear, adhesive film (MicroAmpTM). The plate was transferred to a CLARIOstar multimode microplate reader (BMG Labtech), pre-equilibrated at 30 °C. The plate was incubated for 30 minutes prior to starting measurements to allow equilibration of all samples. Detector gain for parallel and perpendicular channels was adjusted on a 50 nM or 100 nM fluorescent probe mixed in buffer, where the target polarization was set to 10% of the maximum theoretical polarization of fluorescein (350 milli-polarization units). Fluorescence polarization was measured in kinetic mode, every 15 minutes for 800 cycles. Fluorescence polarization (FP) was converted to fluorescence anisotropy (FA) in CLARIOstar MARS software before analysis. All the anisotropy values are reported in millianisotropy (mA) units.

Fluorescence anisotropy oscillator data in Figs. 3 and 4 and Figs. S15-S20 were collected *in vitro* on either a CLARIOstar (BMG) or Spark 10M (TECAN) microplate reader. The fluorescein channel was used for all data collection ($\lambda_{\text{excitation}}$, 482 \pm 8 nm; $\lambda_{\text{emission}}$, 530 \pm 20 nm). Fluorescence anisotropy was monitored from each well in the 384-well plate and recorded every 15 minutes, with time zero representing 3-5 minutes following the addition of KaiC to oscillation reactions. See **Table S4** for specific experimental conditions for each run.

Phosphorylation assays for KaiC and RpaA

For phosphorylation measurements, 250 μ L samples from identical clock reactions were incubated in parallel with the FA experiments and special attention was taken to ensure that phosphorylation reactions were initiated identically to FA reactions by the addition of a solution of KaiC and ATP to a master mix. For detection of RpaA phospho-states, fluorophore-labeled RpaA (50% of total concentration) was used. Samples were incubated at 30 °C in a benchtop water bath. Aliquots (8 μ L) were removed every 4 h by manual pipetting over a period of 72 h. Each aliquot was immediately flash frozen by dipping the tubes in liquid nitrogen and storing at -80 °C until all the aliquots were collected. For phosphorylation analysis, time points were first run on Zn²⁺-Phos-tagTM gels as described below and then the same set of aliquots was run on 7.5% SDS-PAGE for analysis of KaiC~P states.

Sample preparation and analysis on Phos-tag™ gels: Frozen protein aliquots were thawed on ice for 15 minutes and mixed with 8 μL of chilled 2x-SDS-PAGE loading buffer. Samples were spun at 1500 rpm for 30 seconds and transferred quickly to ice. In each lane 4 μL samples were loaded on precast 50 μM -Zn²⁺-Phos-tag™ -12.5% SDS-PAGE gels (Wako Chemicals, Japan). Phosphorylated RpaA was separated by electrophoresis at constant voltage (140 V) for 2 h in freshly prepared 1x running buffer (100 mM Tris, 100 mM MOPS, 0.1% SDS and 5 mM sodium bisulfite, pH 7.8). The electrophoresis apparatus was kept in an ice bath during electrophoresis and running buffer was chilled to 4 °C before use. Fluorescent bands of RpaA were visualized under UV transillumination (E-Gel Imager, Thermo fisher) immediately after electrophoresis was completed and before staining the gels with Coomassie blue protein gel stain.

SDS-PAGE for KaiC phosphorylation: Aliquots prepared for Phos-tag™ gels were saved at -20 °C until analysis. Samples were boiled at 95 °C for 5 min and spun down at 15000 rpm for 30 seconds before loading on 7.5% SDS-PAGE gels. Samples (4 μL) were loaded in each well and two-step electrophoresis was performed at 60 V for 30 min followed by at 140 V for 1 h 40 min. The electrophoresis apparatus was kept in an ice bath and pre-chilled running buffer was used. Gels were stained with InstantBlue® protein gel stain (Expedeon Inc., Novus Biologicals, Centennial Co.) for at least 1 h followed by de-staining in D.I. water for 30 minutes. Gels were imaged by E-gel Imager (Invitrogen, Thermo Fisher Scientific). Densitometry of gel images was performed using NIH ImageJ software (59).

ATPase activity measured by 1H-NMR

A solution of 1.2 μM KaiA, 3.5 μM KaiB, 3.5 μM KaiC, 95% H₂O, 5% D₂O, and 10 μM DSS was prepared in a reaction buffer containing 20 mM Tris, 100 mM NaCl, 1 mM ATP, 5 mM MgCl₂, pH 8. The oscillator reaction was initiated by adding a solution of KaiC and ATP to a solution of KaiA and KaiB. One-dimensional proton NMR spectra were measured at 30 °C, every hour for 5 days. The ATP and ADP peaks were fit using an interpolation function in Wolfram Mathematica. Peak intensities were plotted as function of time and fit to a straight line

from which overall ATPase activity was determined. Oscillations of ATP and ADP resonances about the line provided the determination of ATPase rhythms (see Fig. S6 for details).

Data fitting for phase and period analysis

First 12 h of raw data were removed before analysis because during this time samples are approaching stable limit cycles. Anisotropy and phosphorylation data were baseline-corrected using a quadratic function and normalized to ± 1 before fitting to a damped single cosine function:

$$Y = a \cos\left[2\pi\left(\frac{t}{p}\right) - \phi\right]e^{-kt}$$

where, a = amplitude, p = period, ϕ = phase angle, k = decay constant.

Fluorescence data quantification and statistical analyses in titration experiments: Fluorescence anisotropy readings from clock reactions were collected in MARS Data Analysis Software or SparkControl Software for experiments run on the BMG CLARIOstar Plus or TECAN Spark 10M, respectively. All data were analyzed in the online BioDare suite by FFT-NLLS (60, 61) (<https://biodare2.ed.ac.uk/welcome>). Prior to analysis, fluorescence anisotropy rhythms were baseline detrended and normalized to [-1, 1] with mean of zero. The first 12-h of data were disregarded for quantification of period, amplitude, and phase. Period (**Table S7**) and amplitude (**Table S8**) analysis in **Fig. 3, 4 and S13**, and **S20** were assessed by ordinary one-way ANOVA with Dunnett's multiple comparison tests in Prism 8 (Graph Pad). The significance values and the number of independent experiments for each experimental group are reported in the corresponding figure legends.

Comparisons of the effects of added SasA or CikA on period (**Table S7**) and amplitude (**Table S8**) under different concentrations of the core clock proteins KaiA and KaiB presented in **Table S5** were determined by ordinary two-way ANOVA with Dunnett's multiple comparison tests in Prism 8 (GraphPad). Normalized fluorescence anisotropy rhythms were plotted in conjunction with nonlinear regression least squares cosinor fit in Prism 8 in **Fig. 4**, while raw fluorescence anisotropy data were plotted with Origin Student 2019b (Origin Lab) in **Fig. 3, 4, S13**, and **S20**.

Raw anisotropy data were baseline corrected using an unbound labeled-KaiB reaction well as a reference in each independent experiment.

The damping constant, k , was determined in Prism 8 (GraphPad) using a nonlinear least square regression cosinor fit:

$$y = m * x + amplitude * e^{-kx} * \cos \left[\left(2\pi * \frac{x}{period} \right) + phase \right]$$

where y is the signal, x the corresponding time, amplitude is the height of the peak of the waveform above the trend line, k is the decay constant (such that $1/k$ is the half-life), period is the time taken for a complete cycle to occur and phase is the shift in x relative to a cosinor wave.

Strains and culture conditions for *in vivo* experiments

Synechococcus elongatus PCC 7942 and its derivative strains (Table S12) were maintained on BG-11 medium containing antibiotics as needed for selection (62). Growth on plates or in liquid medium was carried out at 30 °C under 150 $\mu\text{mol m}^{-2} \text{s}^{-1}$ light. *E. coli* DH5 α used for cloning was grown on LB with the appropriate antibiotics at 37 °C.

Construction of rpaA-R121Q strain: Introduction of point mutations into the *S. elongatus* chromosome was accomplished using a previously described CRISPR-editing approach (44). The pSL2680 (Km^R) plasmid used for CRISPR-Cas12a (formerly Cpf1) editing was purchased from Addgene (Plasmid #85581). Primers rpaA_gRNA_F and rpaA_gRNA_R were annealed together and ligated into AarI-cut pSL2680 to serve as the *rpaA-R121Q* gRNA template. The resulting construct was purified and digested with KpnI to facilitate insertion of the *rpaA-R121Q* homology directed repair (HDR) template. The HDR template was generated by amplifying overlapping upstream and downstream fragments using primers rpaA_HDR-UP_F and rpaA_HDR-UP_R (AMC1722 genomic DNA as template) and rpaA_HDR-DWN_F and rpaA_HDR-DWN_R (AMC541 genomic DNA as template), respectively. The upstream and downstream HDR fragments were assembled into KpnI-cut pSL2680+gRNA using the GeneArt Seamless Assembly Kit (Thermo Fisher Scientific), forming pDE32. Plasmid pDE32 was electroporated into *E. coli* DH10B containing a helper plasmid pRL623 (chloramphenicol resistance, Cm^R) and conjugal plasmid pRL443 (ampicillin resistance, Ap^R) (63). The resulting

strain was grown overnight in LB medium containing antibiotics (Ap, kanamycin Km, and Cm), washed 3x with fresh LB, and mixed in a 1:2 ratio with an *S. elongatus* reporter-strain aliquot. The cell mixture was plated onto BG-11 agar with added LB (5% vol/vol), incubated under $100 \mu\text{mol m}^{-2} \text{s}^{-1}$ light for 36 h, then underlaid with Km (10 $\mu\text{g/ml}$ final concentration) to select for *S. elongatus* cells that contain pDE32. Colonies that emerged after 6-8 days were passaged three times on BG-11 agar containing Km to allow editing to occur. Successful editing of chromosomal *rpaA* was verified by sequencing. Plasmid pDE32 was cured from the edited strain by inoculating cells into non-selective BG-11 medium, growing the culture to $\text{OD}_{750} = 0.6$, then dilution plating on non-selective BG-11 plates. Fifty colonies were picked and replica patched to selective (Km) and non-selective medium to identify and isolate clones that had lost pDE32.

Generation of SasA mutants in S. elongatus: Markerless point mutations were introduced in *sasA* of *Synechococcus elongatus* PCC 7942 by CRISPR/Cas12a engineering as previously described (44). Plasmids and the primers used in vector construction and sequence verification are listed in **Table S11 and S12**. Briefly, oligos with complementarity to the guide RNA (gRNA) recognition site were annealed and cloned into AarI-cut pSL2680 (Addgene Plasmid #85581). Clones of pSL2680 that carry the appropriate gRNA insert were isolated and plasmid sequences were verified. Upstream and downstream homologous repair templates that encode the point mutation(s) of interest were amplified by PCR and assembled (GeneArt Seamless Assembly, Thermo Fisher) into KpnI-cut constructs that contain the respective gRNAs. Recovered plasmids were checked for accuracy by Sanger sequencing prior to editing in *S. elongatus*.

The RSF1010-based editing constructs were electroporated into *E. coli* AM1359 that contain conjugal helper plasmids (pRL623 and pRL443) as previously described (64–68). The resulting *E. coli* strains were grown overnight in LB containing ampicillin (100 $\mu\text{g/ml}$), chloramphenicol (17 $\mu\text{g/ml}$) and kanamycin (50 $\mu\text{g/ml}$). Cells from a 1 ml aliquot were washed three times with fresh LB and resuspended in a final volume of 100 μl LB, then mixed with 100 μl of an *S. elongatus* clock-reporter strain (AMC541) concentrated down from 2 ml of a dense culture ($\text{OD}_{750} = \sim 0.6$). The mixed culture was plated to solid BG-11 medium containing 5% LB (v/v) and incubated at 30°C under $30 \mu\text{mol photons m}^{-2} \text{s}^{-1}$ (μE) illumination for 24 hours. Plates were

then underlaid with kanamycin (5 µg/ml final concentration) to select for the editing plasmid. *S. elongatus* colonies that emerged after 8-10 days at 30°C and 100 µE light were serially patched three times to BG-11 containing kanamycin to maintain the editing plasmid long enough to complete segregation of the mutant allele in all copies of the chromosome. After editing, *sasA* was amplified by colony PCR using primers that anneal outside of the homologous repair region and the resulting PCR product was submitted for Sanger sequencing to confirm segregation of the point mutation(s) of interest.

Bioluminescence monitoring of S. elongatus circadian rhythms: Bioluminescence was monitored using a *PkaiBC::luc* firefly luciferase fusion reporter inserted into a neutral site of the *S. elongatus* chromosome as previously described (62). Strains to be monitored were grown in liquid culture to $OD_{750} = 0.4-0.7$, diluted to $OD_{750} = 0.2$, and added as 20 µl aliquots to 280 µl of BG-11 agar containing 3.5 mM firefly luciferin arrayed in 96-well plates. Plates were covered with a gas-permeable seal and cells were entrained under 12-h light-dark cycles ($80 \mu\text{mol m}^{-2} \text{s}^{-1}$ light) to synchronize clock phases. After 48 h of entrainment, cells were released into continuous light ($30 \mu\text{mol m}^{-2} \text{s}^{-1}$) and bioluminescence was monitored every 2 h using a Tecan Infinite Pro M200 Bioluminescence Plate Reader. Mutant *sasA* strains, along with positive and negative clock-output controls, were grown in BG-11 medium, diluted to $OD_{750} = 0.2$ and arrayed in 96-well plates containing solid BG-11 medium and 10 µl of 5 mM D-luciferin. Plates were covered by a gas permeable seal and incubated in a light-dark chamber at 30°C for 48 hours, with 12 h intervals of 120 µE light and darkness. Following release into constant light at the end of 48 hours, plates were transferred to a lighted stacker (40 µE light) attached to a Tecan Infinite M200 Pro and bioluminescence was monitored every 2-3 hours. The raw bioluminescence data were plotted as a function of time (GraphPad Prism 8) and processed using BioDare2 to determine period and amplitude for each set of replicates (61). All strains used in this study are listed in **Table S11**.

Immunoblotting: For detection of RpaA phosphorylation flask-grown cells were collected (15 ml) at ZT 0 and ZT 12 from liquid cultures ($OD_{750} = 0.6-0.7$) incubated under 12-h light-dark cycles ($40 \mu\text{mol m}^{-2} \text{s}^{-1}$). Cells were pelleted, washed once with cold 10 mM sodium chloride

solution and frozen at -80 °C. Cell pellets were thawed on ice and resuspended in tris-buffered saline (pH 7.4) containing 1 mM phenylmethylsulfonyl fluoride, then disrupted by bead beating at 4 °C (30 s of beating, followed by 2 min on ice for 10 cycles). Following centrifugation (20,000 x g for 10 min), protein concentrations were determined by the Bradford assay and a total of 10 µg of protein was loaded per well. Phos-tagTM reagent (20 µM) (Wako Chemicals, Japan) and manganese chloride (100 µM) were added to standard SDS-PAGE gels (12.5 %) to allow detection of phosphorylated RpaA. Electrophoresis was conducted on ice using pre-chilled running buffer to limit hydrolysis of the heat-labile phospho-aspartate. Current was maintained at 25 mA until the bromophenol blue dye reached the bottom edge of the gel. The gel was then incubated for 10 min in transfer buffer containing 10 mM EDTA, followed by a 10 min incubation in transfer buffer without EDTA prior to semi-dry transfer to a PVDF membrane using a Trans-Blot Turbo System (BioRad). Detection of RpaA was achieved using RpaA-antiserum (gift from E. O'Shea, HHMI-Janelia, Ashburn, VA) at a dilution of 1:2000 as described previously (69, 70). Secondary antibody (goat anti-rabbit IgG; 401315, Calbiochem) was used at a dilution of 1:100,000 and chemiluminescent signal was produced using the SuperSignal West Femto Maximum Sensitivity Substrate (Thermo Fisher Scientific).

For detection of total SasA levels protein extraction was performed as described above. Bio-Rad Any kDTM Mini-PROTEAN® TGXTM Precast Protein Gels (cat #4569036) were used to perform SDS-PAGE with 10 µg of protein loaded per well. Detection of SasA was achieved using SasA-antiserum (Aves Lab) at a dilution of 1:4000. Secondary antibody (goat anti-chicken IgY; ab96947, Abcam) was used at a dilution of 1:5000 and chemiluminescent signal was detected by using the SuperSignal West Femto Maximum Sensitivity Substrate (Thermo Fisher Scientific) and imaging with BioRad ChemiDoc system.

Crystallization of monomeric *T. elongatus* C1 domain in complex with *T. elongatus* SasA_{trx}

A monomeric mutant of *T. elongatus* KaiC-CI domain (see **Table S1** for details) was incubated at 250 µM with an excess of *T. elongatus* SasA_{trx} (460 µM) overnight in 20 mM Tris pH 7.0, 150 mM NaCl, 5 mM DTT, 1 mM MgCl₂ and 1 mM ATP at room temperature. The complex was subsequently purified by size-exclusion chromatography on a Sephadex 70 column (GE

Healthcare) equilibrated in the same buffer, but with MgCl₂ and ATP concentrations reduced to 0.5 mM. The complex was mixed in a 1:1 ratio to a final concentration of 10.8 mg/mL with the crystallization buffer containing 1.26 M NaH₂PO₄, 0.54 M K₂HPO₄ (pH unadjusted, total PO₄ concentration 1.8 M), 0.1 M Glycine (added from a 1 M solution adjusted to pH 10.5) and 0.2 M Li₂(SO₄)₂. Crystals formed over 10 days at 22 °C using the hanging drop method. The flat, plate-like crystals were then frozen in liquid nitrogen after soaking in cryoprotectant composed of the crystallization buffer plus 20% (v/v) glycerol.

Structure determination and refinement: Single crystal diffraction data were collected with a wavelength of 1 Å on the 23-ID-D X-ray source at the Advanced Photon Source at the Argonne National Laboratory. Data were processed and scaled using iMOSFLM (71) and Aimless (72). Phases were solved by molecular replacement with the structure of *T. elongatus* KaiC-CI monomer in complex with fsKaiB (PDB 5JWO) using Phaser (73). Refinement and model building were performed using Phenix (74) and Coot (75). See **Table S6** for crystal and refinement statistics. Structural figures were made using UCSF Chimera (76, 77) and ChimeraX (78).

Equilibrium binding assays: Binding titrations were performed in 20 mM Tris pH 7.4, 150 mM NaCl, 1 mM ATP, 1 mM MgCl₂ and 0.1 % (v/v) Tween-20. Fluorescein-labeled KaiB or SasA_{trx} probes were present at 50 nM, while the titrant was diluted serially in 1/3-fold increments. Serial dilutions were performed in a 384-well plate before sealing with tape and incubating at room temperature overnight (9-15 h). Fluorescence polarization anisotropy measurements were subsequently collected on a Synergy2 plate reader (BioTek). Replicate measurements were collected and averaged for each well (20). For 2D titration assays looking at the effect of an additive on KaiB binding to KaiC, fsKaiB or SasA additives were included in both KaiC and diluent buffer to maintain a constant concentration. Diluent was added to the 384-well plate using a single channel pipettor, and additives were mixed into the KaiC stock last and diluted within 10 minutes. See thermodynamic modeling of binding equilibria below for more information.

Thermodynamic modeling of binding equilibria: The fluorescence anisotropy titrations outlined above involve cooperative and competitive reactions and span a wide range of concentrations,

such that free ligand concentrations cannot be approximated by the total added concentration. Consequently, these data cannot be analyzed by fitting to standard analytical equations (79). Fitting the data to the profiles simulated by a model avoids this problem but introduces others in terms of the complexity of the model that is required for the fit. Initially, we attempted to fit to a general hexameric model for KaiC but found there were too many parameters to reach convergence. When simplified to a dimer model, the fits were reasonably robust and showed no systematic deviations. Nevertheless, such a simplified model required positive heterotropic or homotropic cooperativity between KaiB and additives such as SasA and fsKaiB, respectively, as well as competition between these additives. Thus, a dimer model captures the essence of the interaction, although how this relates in detail to cooperativity within the KaiC hexamer remains in question.

Least-squares fitting analysis to models was performed using DynaFit (BioKin) (80). Scripts used for analysis are available in supplemental data (**Data 1** and **2**). Statistical analysis was performed using the Monte Carlo routine. Cooperativity indices (described by $K_1/K_3 = K_2/K_4$, see **Data S3**) were calculated for each simulation ($n = 1000$) and median and 95% confidence intervals taken as ranks 500, 25 and 975 (respectively) in the $n = 1000$ simulation. Where replicate measurements are reported, the values of median or 95% confidence boundaries were averaged amongst the replicates.

In order to reduce the number of parameters of the fit, the binding of KaiB alone was initially modeled without any homotropic cooperativity by assigning $K_5 = 4 * K_1$, as is appropriate for the macroscopic equilibrium constants for two-site independent binding. When K_5 was floated, a slightly improved fit was obtained with a returned $K_5 < K_1$, indicative of homotropic cooperativity, but K_5 was not robustly defined. The value of the heterotropic cooperativity index in the presence of additives increased when K_5 was floated, however, we report fits where K_5 was defined as $4 * K_1$ for simplicity, which gives a minimal estimate of the heterotropic cooperativity index. The input and output files from the least-squares fitting and Monte Carlo analysis are available as **Data S3**. Input KaiC dimer concentrations are given in Data S3, while KaiC concentrations given in terms of total monomer elsewhere.

Triplicate 2D titrations were collected with SasA to optimize the analysis and showed some variability that was ameliorated by floating additive concentrations at the 3 highest additive concentrations. The averages from these fits were used for SasA and KaiB variant 2D titration datasets when analyzing 300 nM data, where additive concentrations were also allowed to float. Little variation was seen in the experimental anisotropy values determined for fluorescently labeled KaiB alone or the final peak values for the KaiB-KaiC complex, though the average peak experimental anisotropy values of putative ternary complexes seeded by heterocooperativity differed modestly between the SasA and fsKaiB variants (KaiB peak anisotropy = 0.211 for SasA or 0.205 for fsKaiB).

Size-exclusion chromatography-multiangle light-scattering (SEC-MALS) assays: SEC-MALS assays were performed at room temperature using a silica-based size-exclusion column (particle size 5 μm , pore size 500 Angstrom, 4.6 mm ID, Cat. No. WTC-050N5, Wyatt Technologies) to resolve the oligomeric state of SasA. 20 μL injections of full-length SasA at 1.5 mg/mL were made using an Agilent G1311A quaternary pump and manual injector (Rheodyne), run over the silica-based column, and analyzed by a T-rEX refractometer and miniDAWN TREOS II static multiangle light scattering instrument (Wyatt Technologies) directly after the column. Analysis of absolute molecular weight was carried out using Astra 6.0 software (Wyatt Technologies).

³²P phosphotransfer assay

Assays were performed in the presence of γ -³²P ATP as originally described (19). These experiments were conducted with 5 μM KaiC-EE, 3.5 μM RpaA, and 2.5 μM SasA variant in 0.1 mM ATP. To do this 100 μM KaiC in 1.0 mM ATP was diluted with 20 mM Tris pH 7.4, 150 mM NaCl, 1 mM MgCl₂, 1 mM TCEP. 4 μL of undiluted γ -³²P ATP (EasyTides).

SasA-WT and SasA-DM were compared in this assay by quenching the reactions at discrete timepoints using an equivalent volume of 6x SDS-PAGE loading buffer. ³²P labeled protein was separated on an anyK_DTM pre-cast SDS-PAGE gel (BioRad). Gels were dried and exposed overnight for visualization on a Typhoon phosphorimager, and subsequent quantification by densitometry. Slopes of the resulting trajectories were compared in triplicate between wild-type SasA and SasA-H28A-Q94A to determine the % activity the double mutant. A control was also

included where no RpaA was added to quantify the efficiency of initial histidine phosphorylation to the SasA variants, and triplicate densitometries were compared at a single timepoint.

Supplementary Data and Figures

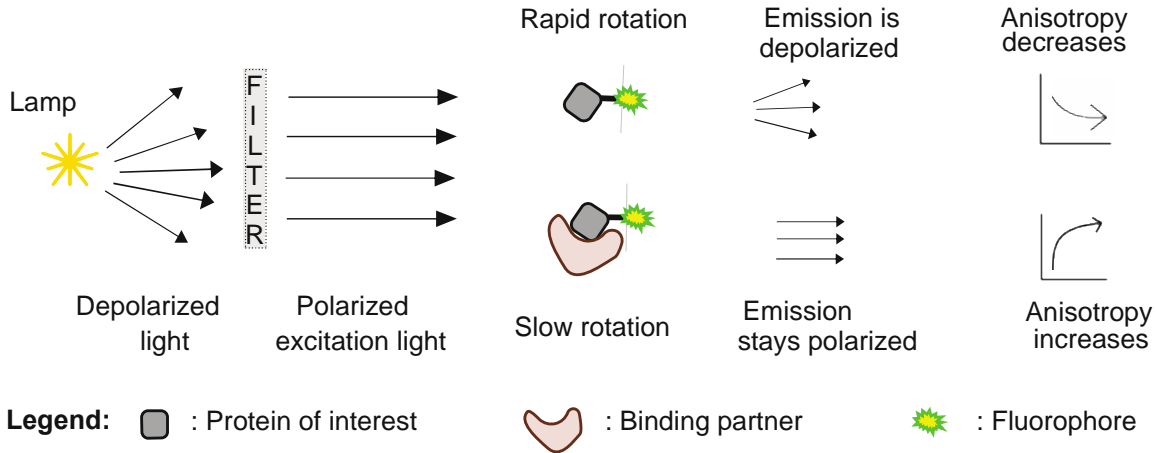


Figure S1: A schematic of fluorescence anisotropy (FA) assay used for real-time monitoring of rhythmic protein-protein interactions in IVC.

Fluorescence anisotropy occurs through excitation of a fluorescently labeled protein of interest. When the protein of interest is not part of a high molecular weight complex, its rotational correlation time is generally shorter than the fluorescence lifetime of the fluorophore, resulting in depolarized emission which can be quantified as lower anisotropy. Upon binding to its partner, the rotational correlation time of the labeled protein of interest increases, resulting in more polarized emission and a higher anisotropy value.

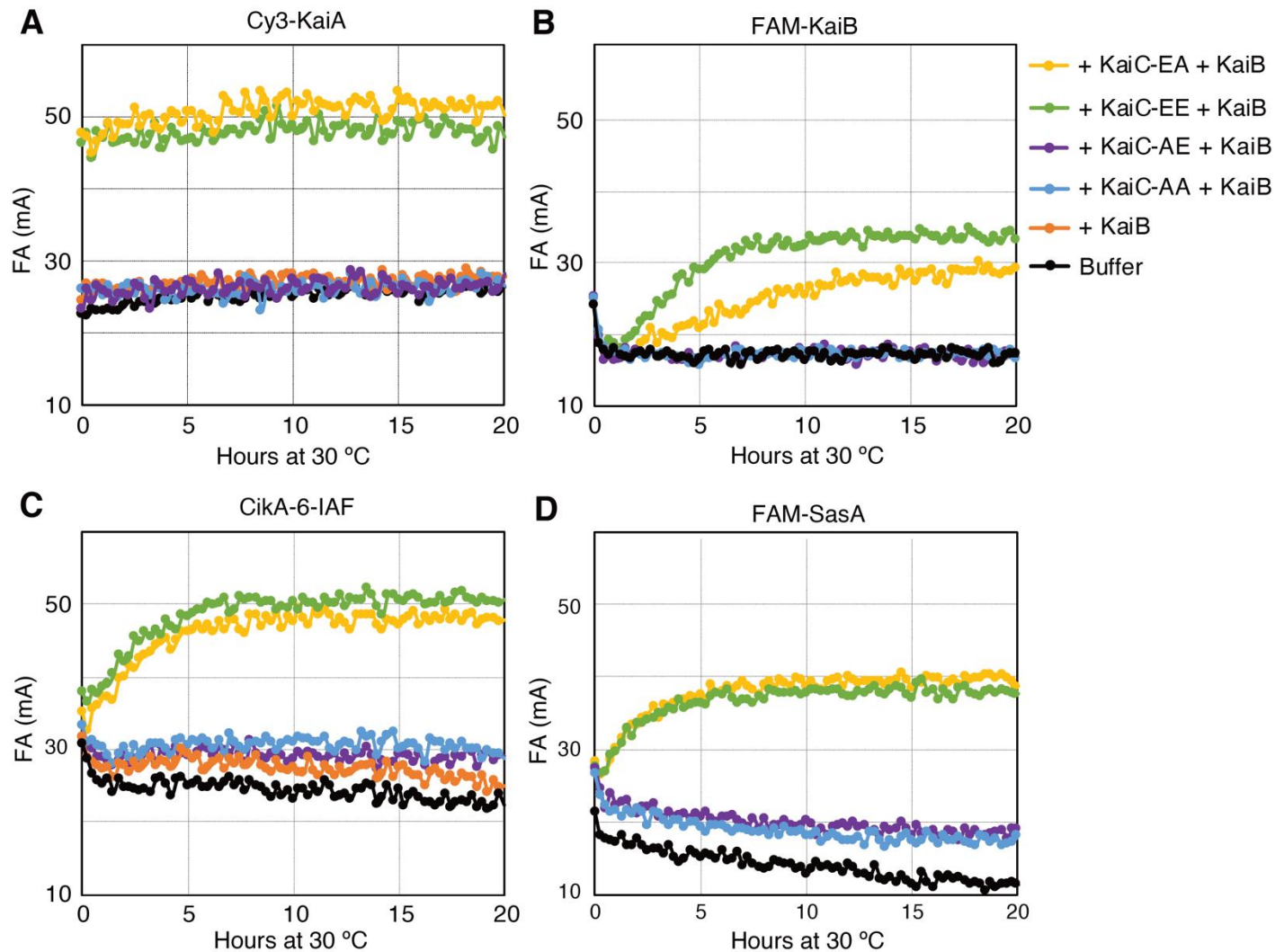


Figure S2. Fluorescence anisotropy of KaiA, KaiB, CikA, and SasA in partial clock reactions.

Control experiments of fluorescence anisotropies (FA) of labeled clock proteins at 50 nM were incubated with 3.5 μ M KaiB (orange), or a mixture of 3.5 μ M KaiB with a separate 3.5 μ M KaiC phosphomimetics. Anisotropies of each labeled protein mixed with buffer are shown in black. The four phospho-states of KaiC can be mimicked by mutating S431 and T432 to either Ala or Glu (8). These phosphostates are indicated as KaiC-AA (S431A, T432A, blue), KaiC-AE (S431A, T432E, violet), KaiC-EE (S431E, T432E, green) and KaiC-EA (S431E, T432A, yellow). KaiC-EE and KaiC-EA respectively approximate the dusk pS,pT and nighttime pS,T states of KaiC. **(A)** Cy3-KaiA: G-KaiA was labeled at the N-terminus with C-(Cy3)-LPETGG **(B)** FAM-KaiB: G-KaiB was labeled at the N-terminus with 5-FAM-LPETGG **(C)** CikA-6-IAF: CikA-LPETG was labeled at the C-terminus with GGGYC-(6-IAF)N, shows binding to KaiB

only in presence of KaiC-EA/EE and **(D)** FAM-SasA: G-SasA was labeled at the N-terminus with 5-FAM-LPETGG and shows increased anisotropy in presence of KaiC-EE/EA. **(A and C)** shows that KaiA and CikA anisotropies report their binding to KaiB in presence of KaiC-EE or KaiC-EA, suggesting nighttime ternary complex formation and is consistent with the peak anisotropies observed for KaiA and CikA in IVC that peaks with KaiB anisotropy **(Fig. 2)**. **(B and D)** Shows that SasA and KaiB both bind to hyperphosphorylated KaiC (KaiC-EE/EA) at dusk. Difference in binding kinetics of SasA and KaiB is also consistent with phase difference observed in IVC **(Fig 1)**.

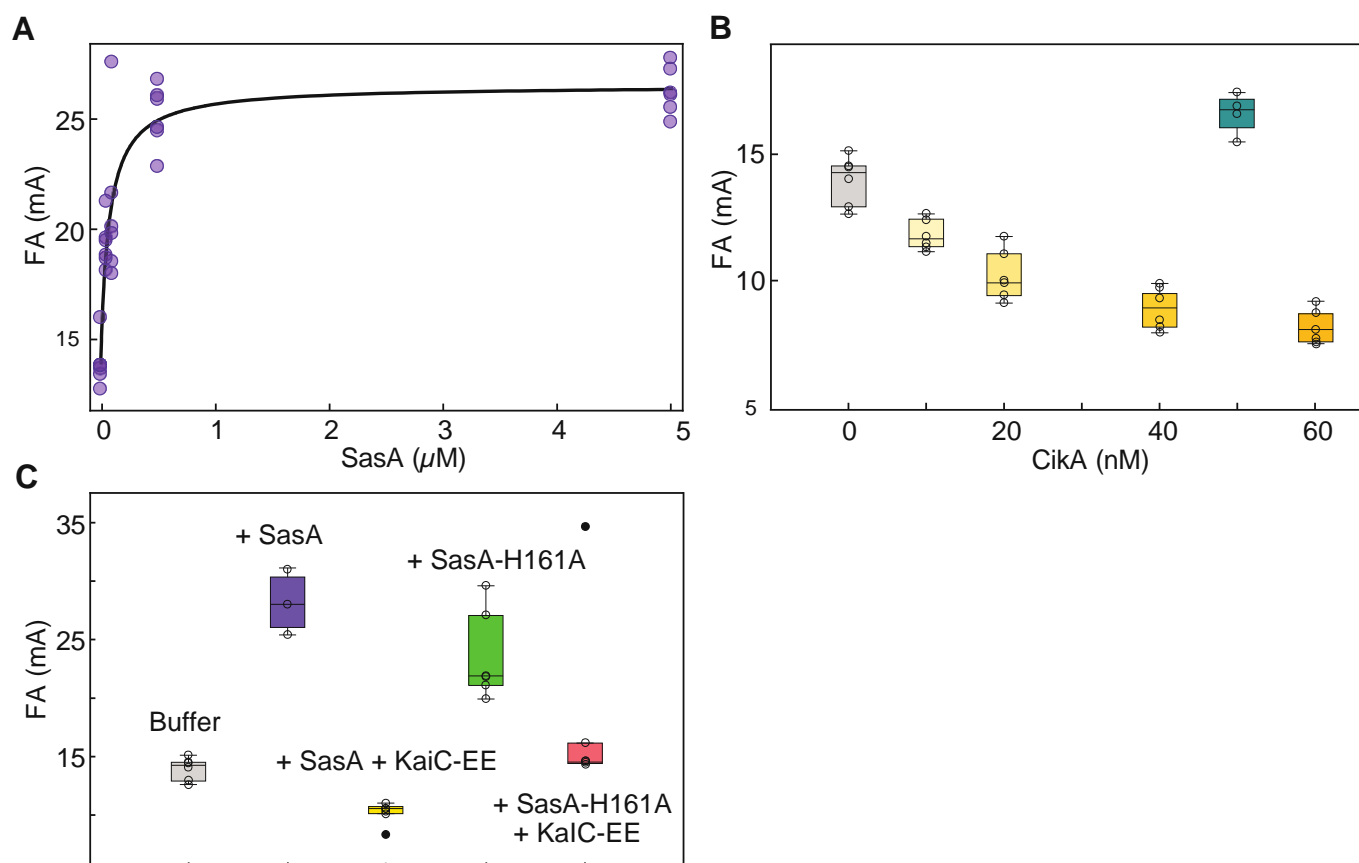


Figure S3. Fluorescence anisotropy of RpaA in the presence of SasA and CikA.

FAM-labeled RpaA (50 nM) was incubated at 30 °C with various amounts of (A) SasA or (B) CikA. Reported fluorescence anisotropies were measured when the reactions reached steady state. (A) Fluorescence anisotropies of 50 nM FAM-labeled RpaA from six replicates are plotted as a function of SasA concentration (purple circles) and data for each replicate were separately fit to the following equation (81):

$$FA = FA_i + (FA_{max} - FA_i) \left(\frac{[SasA]}{[SasA] + K_D} \right)$$

where, FA = fluorescence anisotropy of RpaA,

FA_i = initial fluorescence anisotropy of RpaA,

FA_{max} = maximum fluorescence anisotropy of RpaA,

$[SasA]$ = concentration of SasA (μM),

K_D = apparent dissociation constant (μM).

(A) Fitting the six data sets separately, the average apparent dissociation constant (K_D) is $0.07 \pm 0.02 \mu M$. (B) Box and whisker plots for RpaA fluorescence anisotropies measured from six

replicates as a function of CikA concentration (light to dark yellow), and also when separately incubated with 50 nM of CikA-H393A (teal, 4 replicates). RpaA alone is shown in gray. (C) Box and whisker plots for fluorescence anisotropies from six replicates of RpaA alone (gray), when incubated with 0.65 μ M SasA (purple, 3 replicates), 0.65 μ M SasA-H161A (green), 0.65 μ M SasA + 3.5 μ M KaiC-EE (yellow), or 0.65 μ M SasA-H161A + 3.5 μ M KaiC-EE (pink). The whisker fences denote minimum and maximum values in the data sets, excluding outliers, while the bottom and top of a box represent the first and third quartiles, respectively. A horizontal black line inside the box denotes the median. Individual data points are shown with open circles and outliers are shown as filled black circles. RpaA anisotropy decreases in presence of SasA+KaiC-EE or CikA, suggesting that phosphorylation of RpaA results in decrease in RpaA anisotropy. Kinase-dead mutants of SasA (H161A) and of CikA (H393A) serve as negative controls to show that RpaA anisotropy remains high in absence of phosphorylation.

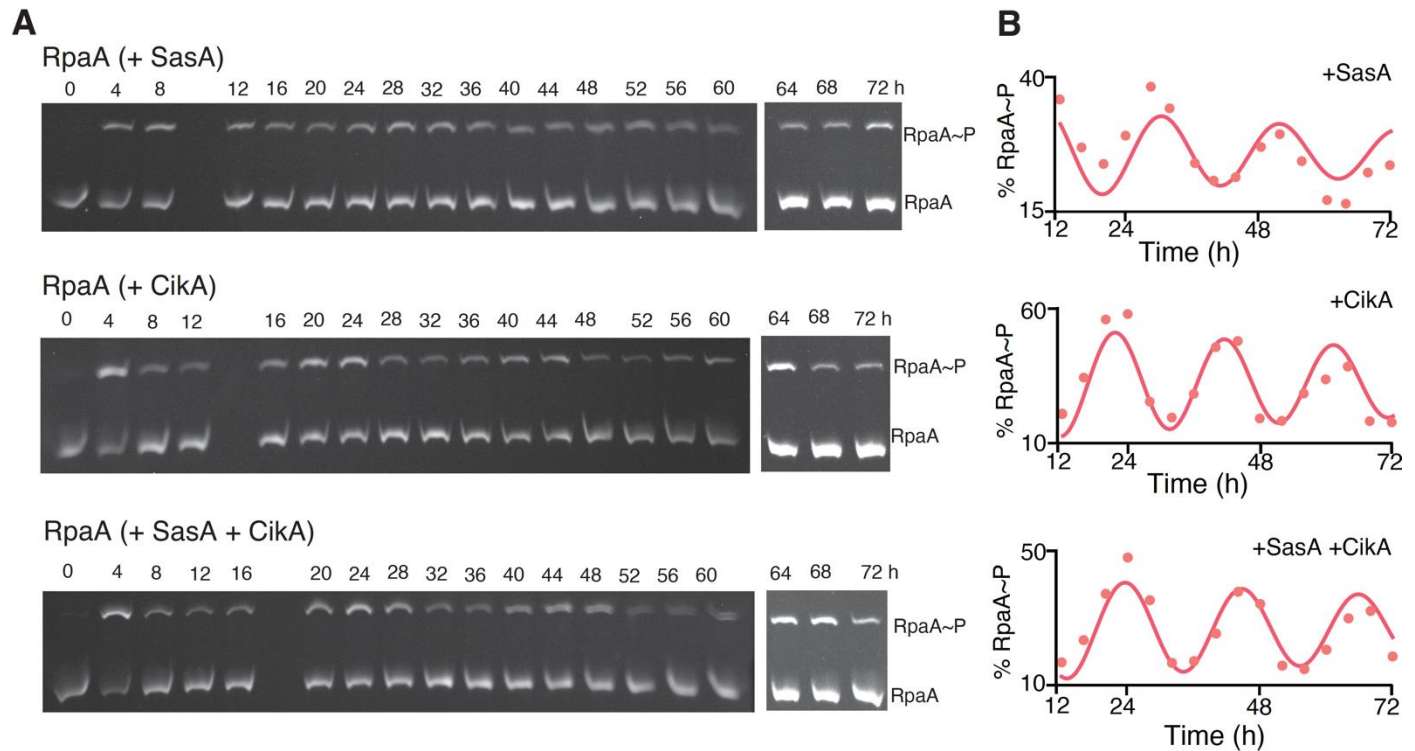


Figure S4. Phos-tagTM SDS-PAGE for WT RpaA phosphorylation *in vitro*.

(A) Aliquots of reconstituted clock reactions containing KaiA, KaiB, KaiC, RpaA, DNA, and either SasA, CikA, or both were sampled every 4 h manually, subjected to 12.5% Zn²⁺ Phos-tagTM SDS-PAGE, and visualized by UV-transillumination (see Materials and Methods for details). (B) Densitometry of the gels was performed by ImageJ (NIH) and band intensities were used to determine the level of RpaA phosphorylation at each time point using the equation

$$\%RpaA\sim P = 100\% * RpaA\sim P / (RpaA + RpaA\sim P)$$

Top, middle, and bottom panels are from IVC reactions that used SasA, CikA, and SasA + CikA.

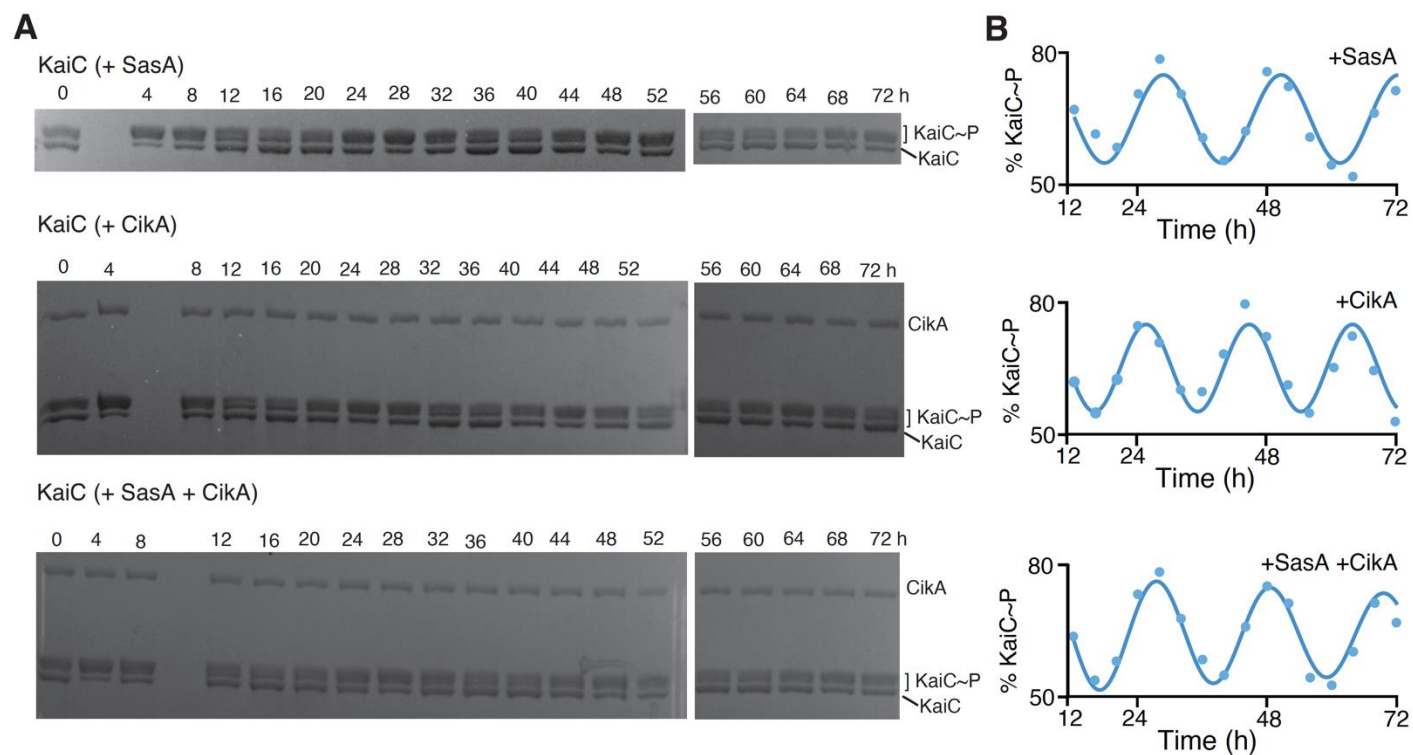


Figure S5. SDS-PAGE of KaiC phosphorylation *in vitro*.

KaiC~P was measured in IVC reactions containing KaiA, KaiB, KaiC, RpaA, DNA, and either SasA (top), CikA (middle), or both SasA and CikA (bottom). (A) Aliquots were collected every 4 h, subjected to 7.5% SDS-PAGE, and stained with Instant Blue (Expedion) dye. The gels were analyzed by ImageJ software (NIH), where the sum of intensities of the top three bands were used to calculate the level of phosphorylated KaiC (KaiC~P). The bottom band is of unphosphorylated KaiC. (B) $\% \text{KaiC~P} = \text{KaiC~P} / \text{total KaiC}$ is plotted as function of time where top, middle, and bottom panels are from IVC reactions that used SasA, CikA, and SasA + CikA.

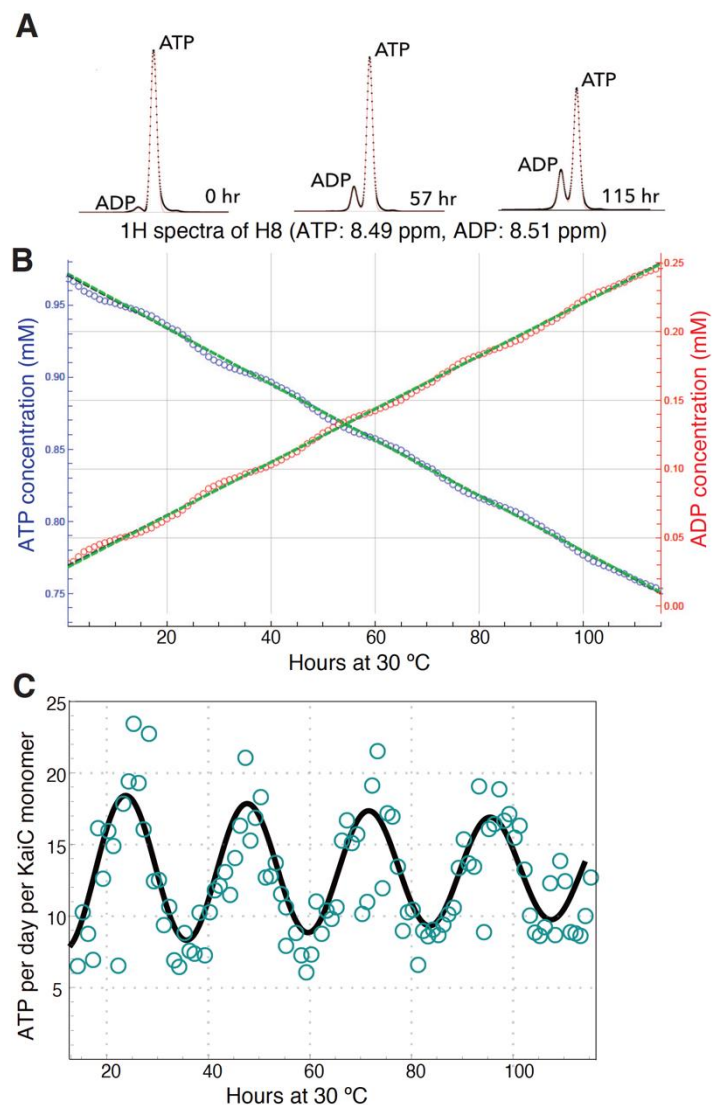


Figure S6. ^1H NMR of ATP and ADP in a KaiABC oscillator reaction.

(A) H8 protons on the adenosine rings of ATP and ADP with chemical shifts of 8.49 ppm and 8.51 ppm, respectively, were monitored by ^1H NMR as a function of reaction time. One-dimensional spectra were collected every hour and changes in peak intensities were measured.

(B) Based on total nucleotide concentration of 1 mM, integrated peak intensities of ATP (blue) and ADP (red) at each time point were converted to concentrations in mM. The green lines are linear fits through the data.

(C) ATPase activity is shown by teal circles and a cosine fit is shown in black. ATPase activity oscillated between 8-18 ATPs per day per KaiC monomer. During the first 12 hours, the sample was approaching a stable limit cycle and thus this data was not used in the fit. In a second measurement oscillations were between 7-13 ATPs per day per KaiC monomer.

Figure S7. Enzymatic activities of SasA and CikA in partial clock reactions.

(A) Schematics for RpaA phosphorylation assay in the presence of CikA (left panel) and SasA + KaiC-EE (right panel). 2.5 μM FAM-RpaA was incubated with either 0.65 μM CikA or a mixture of 0.65 μM SasA and 3.5 μM KaiC-EE at 30 $^{\circ}\text{C}$ in a buffer containing 1 mM ATP and 5 mM MgCl_2 , pH 8. In the left panel an aliquot was removed immediately after RpaA and CikA were mixed ($t = 0$ h). The reaction was incubated at 30 $^{\circ}\text{C}$ for 6 h then divided into two equal portions, one portion received an equal volume of buffer and other received a pre-incubated mixture of KaiB + KaiC-EE (3.5 μM each). Aliquots were taken from both tubes immediately after mixing ($t = 6$ h). Incubation continued at 30 $^{\circ}\text{C}$ for an additional 6 h at the end of which aliquots were removed from each tube ($t = 12$ h). In the right panel, FAM-RpaA was mixed with SasA and KaiC-EE. An aliquot was removed immediately after mixing ($t = 0$ h). After incubating for 6 h at 30 $^{\circ}\text{C}$ the sample was divided into two separate tubes. One tube received buffer and other tube received 3.5 μM KaiB after which aliquots were immediately taken ($t = 6$ h). Both samples were further incubated for 6 h at 30 $^{\circ}\text{C}$ at the end of which aliquots were removed from each tube ($t = 12$ h). Time points for control reactions containing FAM-RpaA (Control-1), FAM-RpaA + SasA (Control-2) or FAM-RpaA + KaiC-EE + KaiB (Control-3) were also collected. (B) Aliquots were loaded onto 12.5% Zn^{2+} -Phos-tagTM SDS-PAGE for separation of RpaA phosphoforms. Coomassie blue-stained gel is in the top panel. Fluorescently labeled RpaA (FAM-RpaA) bands were visualized under UV transillumination (bottom panel). %RpaA~P was determined by densitometry.

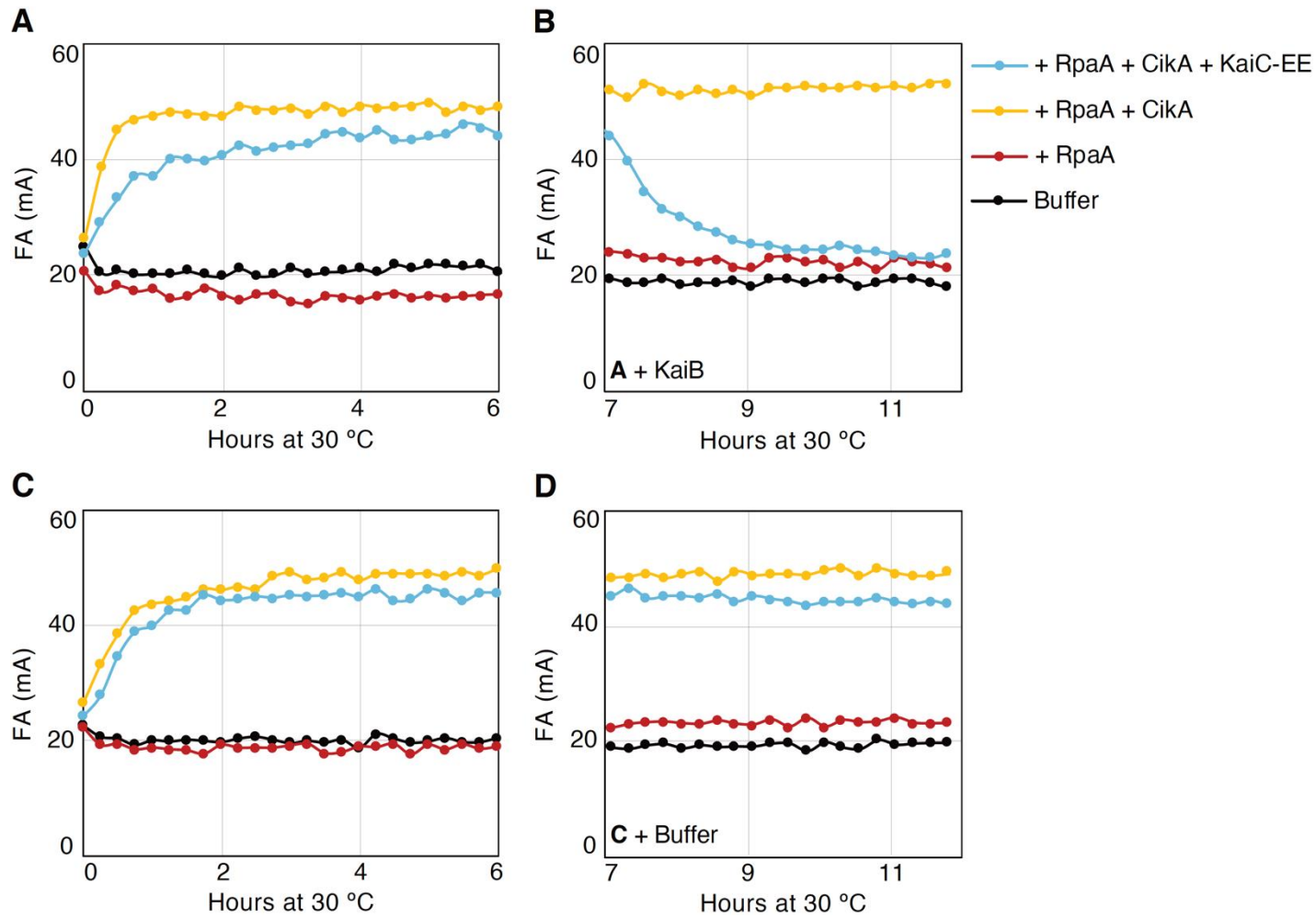


Figure S8. Kinase and phosphatase activity of Cika assessed by DNA binding in vitro.

Fluorescence anisotropies of 100 nM Cy3-labeled *PkaiBC* DNA was measured in buffer containing 1 mM ATP and 5 mM MgCl₂, pH 8. (A) *PkaiBC* alone (black), *PkaiBC* + RpaA (red), *PkaiBC* + RpaA + Cika (yellow), and *PkaiBC* + RpaA + Cika + KaiC-EE (light blue). (B) KaiB was added to samples in (A). (C) Replicate of (A). (D) Buffer was added to samples in (C). After addition of KaiB or buffer at $t = 6$ h, samples were incubated for 1 h before measuring anisotropies for another 5 h. Sample concentrations were 2.5 μ M RpaA, 0.65 μ M Cika, 3.5 μ M KaiB, and 3.5 μ M KaiC-EE.

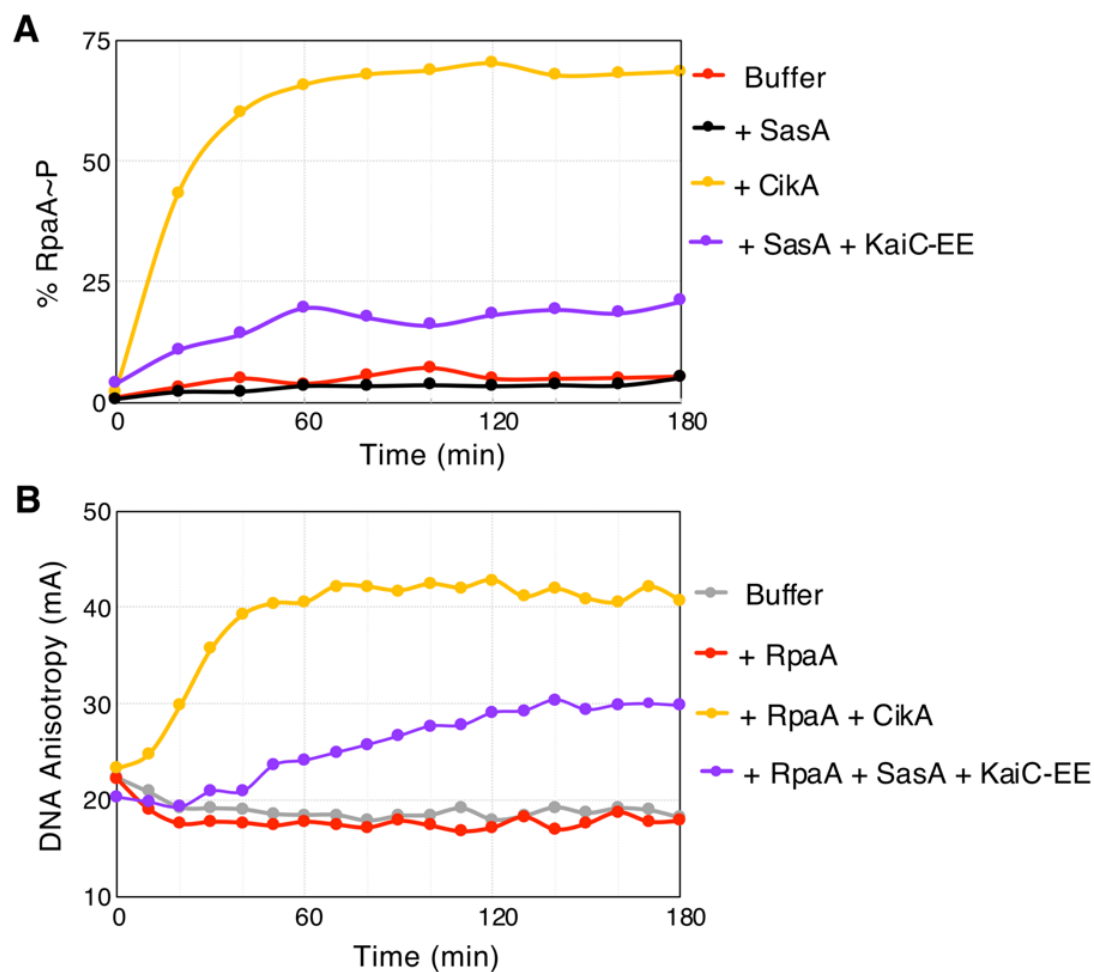


Figure S9. Differential kinetics of SasA and CikA activities produce phase offset in RpaA~P and DNA rhythms.

(A) Rates of RpaA phosphorylation measured in just buffer (red) and in the presence of SasA (black), CikA (yellow), and SasA+KaiC-EE (purple). (B) Fluorescence anisotropy of Cy3-labeled *PkaiBC* DNA measured in just buffer (grey) and in the presence of RpaA (red), RpaA+CikA (yellow), and RpaA+SasA+KaiC-EE (purple). Concentrations of proteins used are: RpaA: 2.5 μ M, CikA: 0.65 μ M, SasA: 0.65 μ M, KaiC-EE: 3.5 μ M and Cy3-*PkaiBC*: 100 nM.

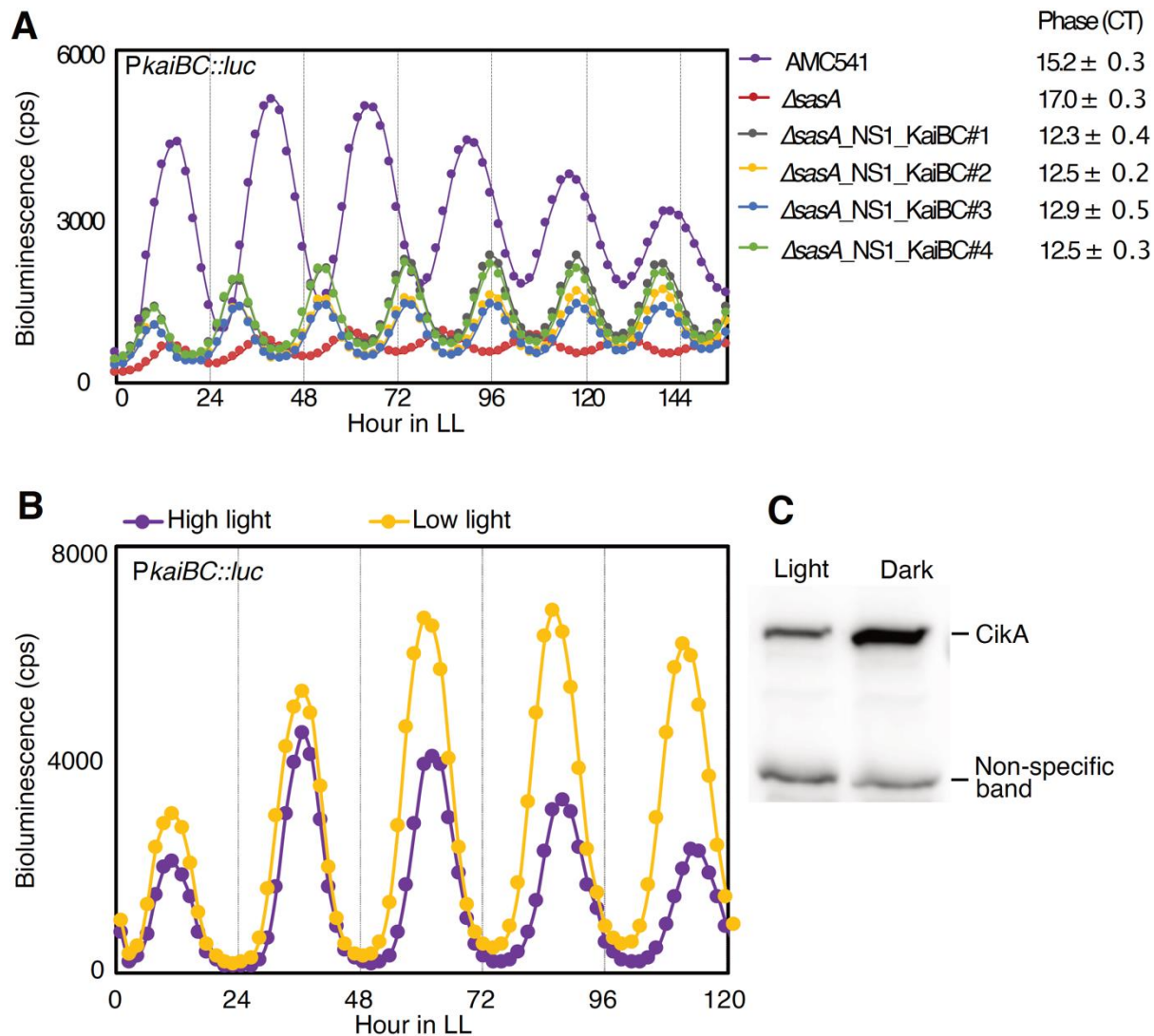


Figure S10. Bioluminescence rhythms of *PkaiBC* in a $\Delta sasA$ background.

(A) Expression from *PkaiBC* monitored as bioluminescence from a *PkaiBC::luc* firefly luciferase reporter. Bioluminescence is nearly arrhythmic in a $\Delta sasA$ mutant (red) as compared to WT strain (AMC541, purple). When *kaiBC* was driven by an *E. coli* promoter, *P_{trc}* (20), in a $\Delta sasA$ background to restore wild-type levels of KaiBC, rhythms were restored with ~3-h phase advance as compared to WT (traces from 4 replicates shown). (B) Rhythms of bioluminescence generated by *PkaiBC::luc* expression were monitored for entrained wild type (AMC541) in high light (purple) or low light (yellow) conditions. (C) CikA levels in AMC06 were probed using anti-CikA serum in cells grown in light or dark. Culture from one flask was split and kept under light or dark conditions for 6 h before harvesting. A more detailed analysis on CikA level under light/dark conditions can be found in Ivleva et al. (38).

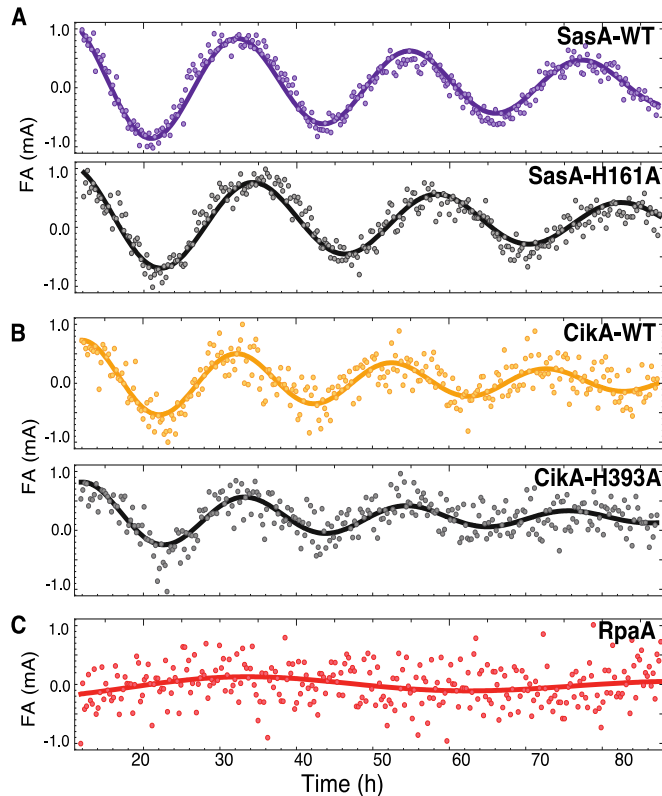


Figure S11: Fluorescence anisotropy rhythms of SasA and CikA kinase dead mutants in an IVC.

(A) Fluorescence anisotropy of SasA-WT (purple) and SasA-H161A (black) probes in an IVC containing KaiA, KaiB, and KaiC and unlabeled WT or mutant SasA. (B) Fluorescence anisotropy of CikA-WT (yellow) and CikA-H393A (black) probes in an IVC containing KaiA, KaiB, and KaiC and unlabeled WT or mutant CikA. Rhythmicity in fluorescence anisotropy for both WT and mutants of SasA and CikA suggesting their interaction with the core clock are unaffected by the mutations. RpaA~P and DNA fluorescence anisotropy showed no rhythmicity in IVC containing SasA-H161A or CikA-H393A mutants, suggesting phosphorylation dependent interaction of RpaA and DNA. (C) Fluorescence anisotropy of labeled RpaA (red) in core oscillator reaction containing KaiA, KaiB and KaiC, but no SasA or CikA, has no rhythmicity of interaction with core clock proteins.

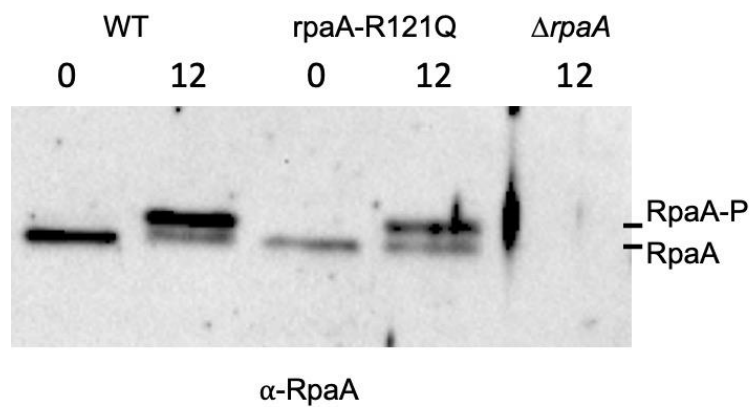


Figure S12. RpaA-R121Q mutant shows WT-like phosphorylation pattern *in vivo*.

Phos-tagTM immunoblots reveal the level of RpaA phosphorylation in entrained wild-type, and *rpaA-R121Q* cells at ZT = 0 (dawn) and ZT = 12 (dusk). A sample from a Δ rpaA strain is included as a negative control. Each lane contains 10 μ g of total protein.

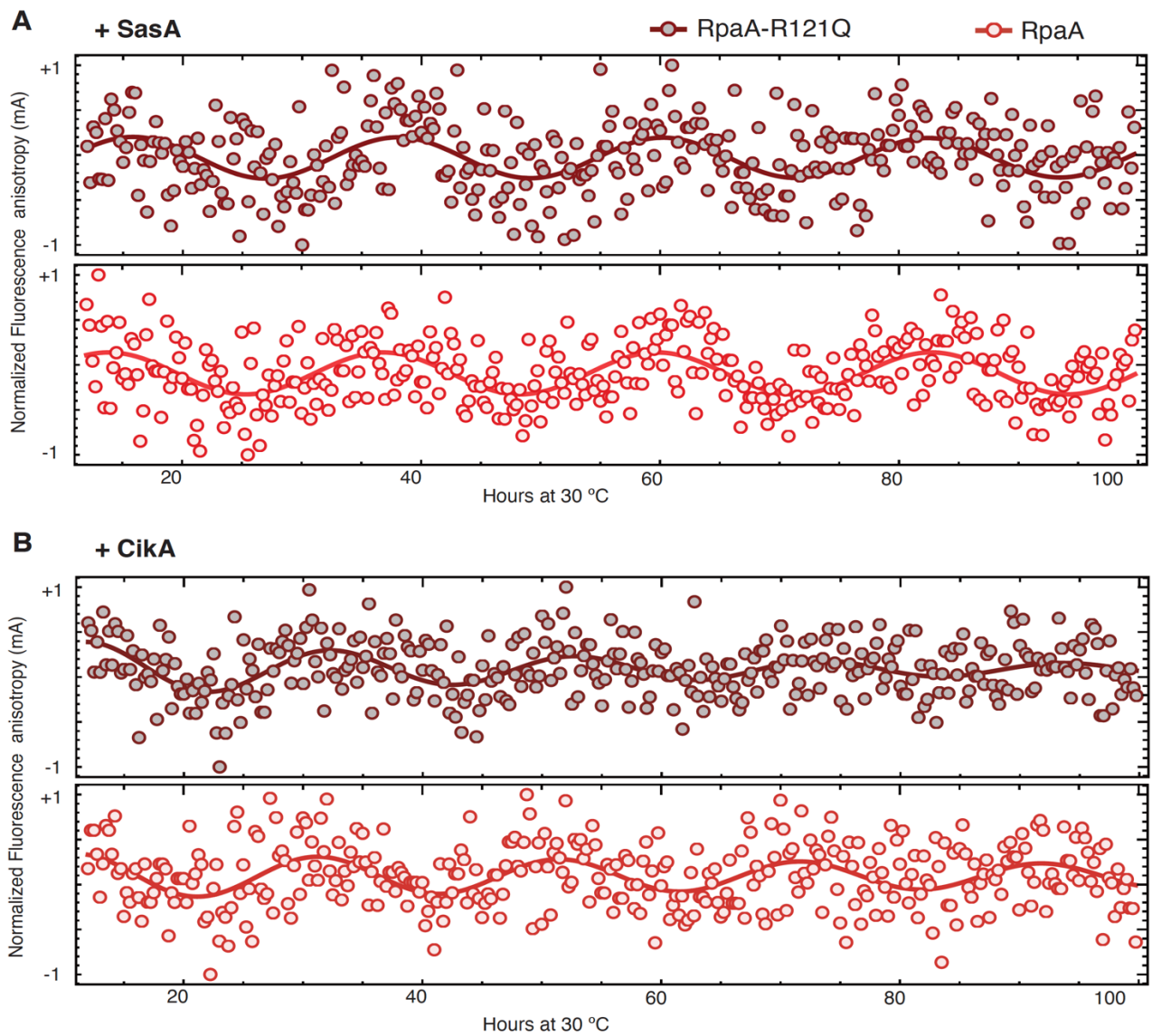


Figure S13. RpaA and RpaA-R121Q fluorescence anisotropy in IVC.

Fluorescence anisotropy rhythms of labeled FAM-RpaA (red) and FAM-RpaA-R121Q (brown), measured in IVC containing KaiA, KaiB, KaiC and 0.65 μ M of either (A) SasA or (B) Cika.

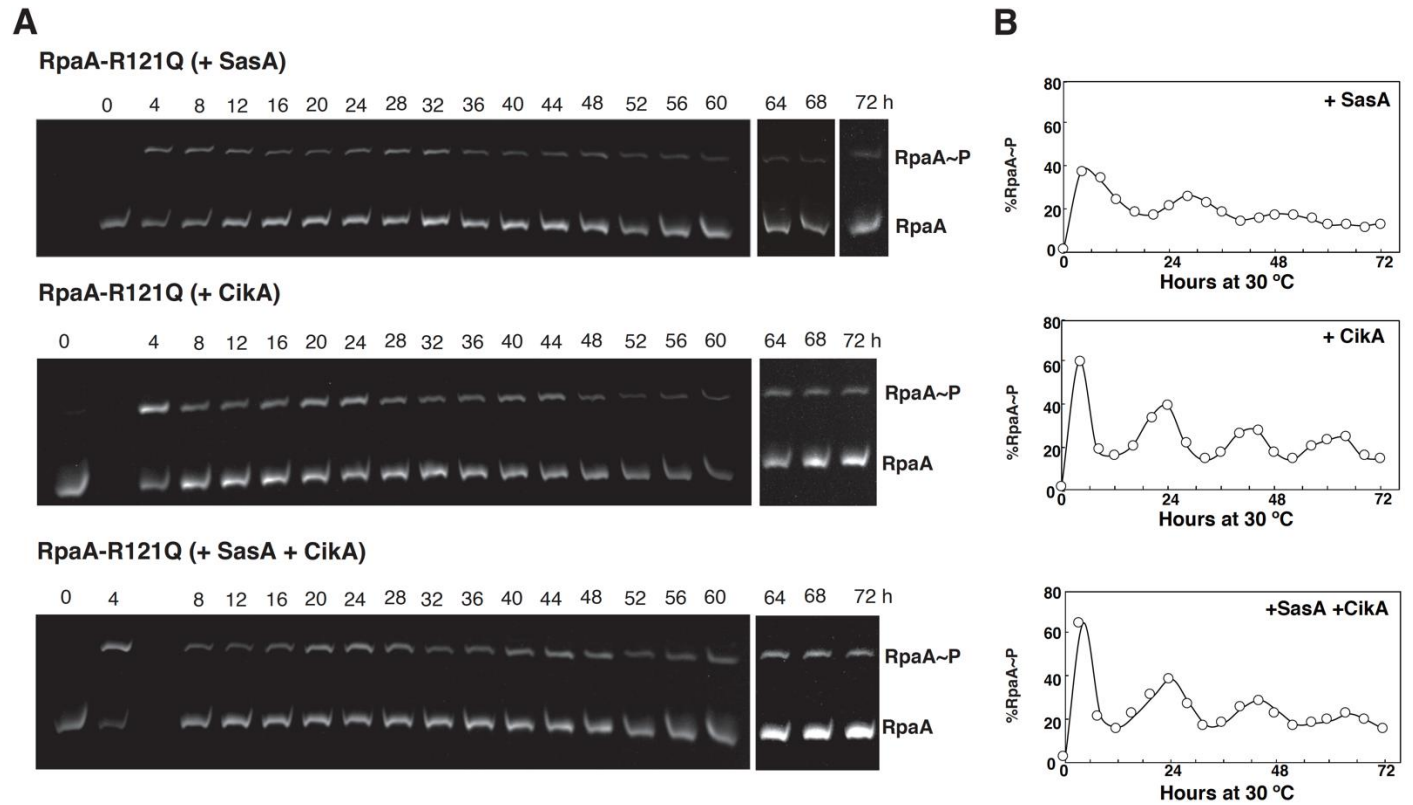


Figure S14. Phos-tagTM SDS-PAGE of RpaA-R121Q phosphorylation in vitro.

(A) Aliquots of reconstituted clock reactions containing KaiA, KaiB, KaiC, RpaA-R121Q, DNA, and either SasA (top), CikA (middle), or both (bottom) were sampled every 4 h manually, subjected to 12.5% Zn²⁺ Phos-tagTM SDS-PAGE, and visualized by UV-transillumination (see Materials and Methods for details). (B) Densitometry of the gels was performed by ImageJ (NIH) and %RpaA~P = 100% * RpaA~P / (RpaA + RpaA~P) is plotted as function of time.

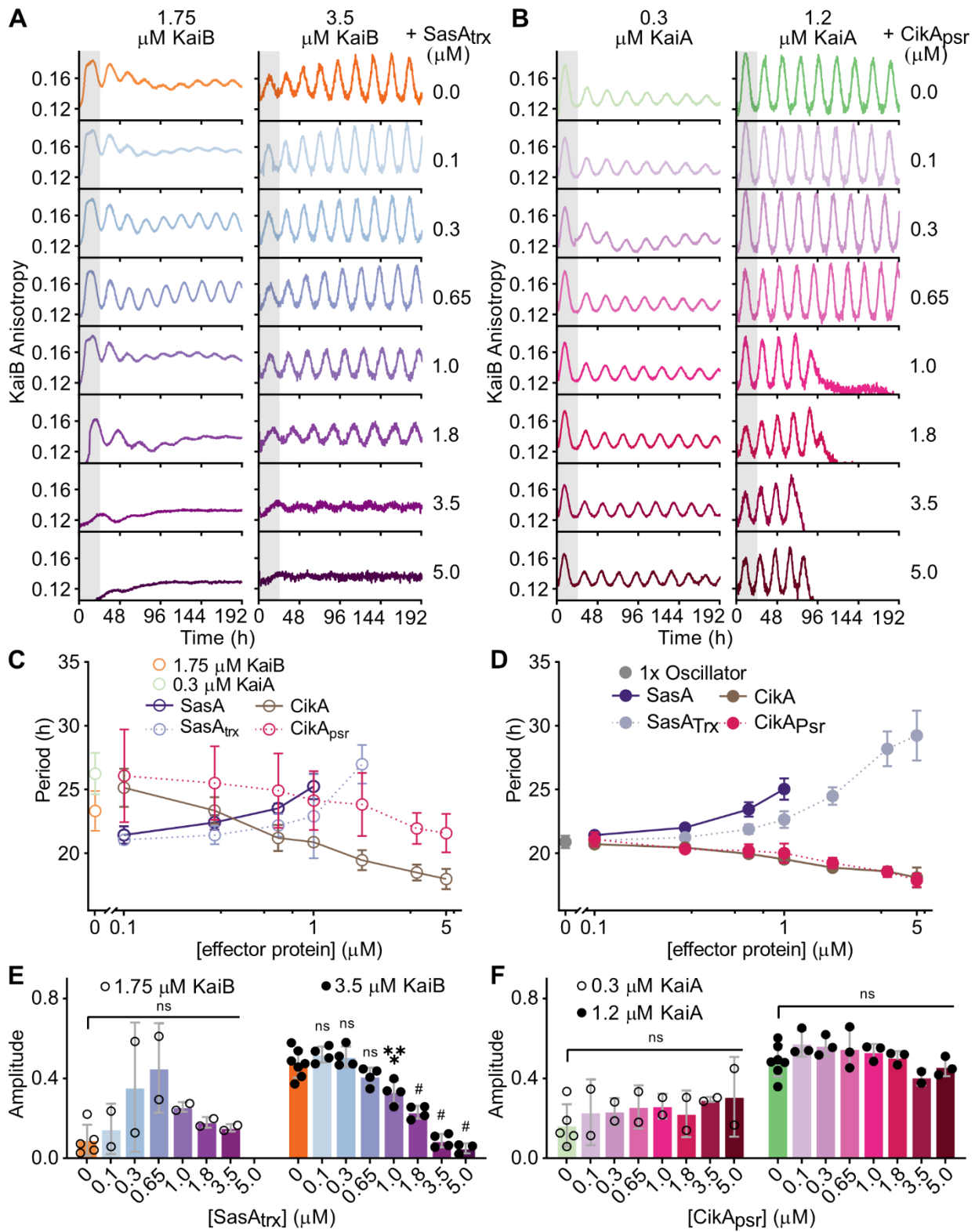


Figure S15. Domain truncation studies on SasA and CikA oscillator effects.

(A-B) Fluorescence assays under conditions of 3.5 μM KaiC, 50 nM fluorescently labeled KaiB as a probe, and either (panel **A**) standard 1.2 μM KaiA with 1.75 μM or 3.5 μM KaiB, or (panel **B**) standard 3.5 μM KaiB with 0.3 μM or 1.2 μM KaiA as indicated with titrations of truncated domain (panel **A**) SasA_{trx} or (panel **B**) CikA_{psr} from 0.1 – 5.0 μM . Representative assay from $n \geq 2$ shown; the first 24-h period after release into constant conditions is marked in gray. **(C-D)** Period values for fluorescence assays prepared with deficient (panel **C**) 1.75 μM KaiB and (panel **D**) 0.3 μM KaiA (open circles) or standard oscillator concentrations (panel **C**) 3.5 μM KaiB and (panel **D**) 1.2 μM KaiA (closed circles) in the absence and presence of full-length (solid connecting lines) and truncated additive proteins (dotted connecting lines). Period and amplitude data are representative of one or more independent experiments with duplicate samples, presented as the mean \pm SD. **(E-F)** Amplitude for fluorescence assays prepared under different core KaiB and KaiA concentrations of (panel **E**) deficient (open circles) or (panel **F**) standard (closed circles) in the absence or presence of truncated additive proteins. Data are shown as mean \pm SD ($n \geq 2$ with duplicate samples). Analysis of variance (ANOVA) was used to compare amplitudes of fluorescence anisotropies under the two KaiB and KaiA concentrations in the absence of truncated domains SasA_{trx} and CikA_{psr}, respectively, versus the indicated concentrations of those additive proteins: ns, not significant; *, $P < 0.05$; **, $P < 0.01$; ***, $P < 0.001$; #, $P < 0.0001$.

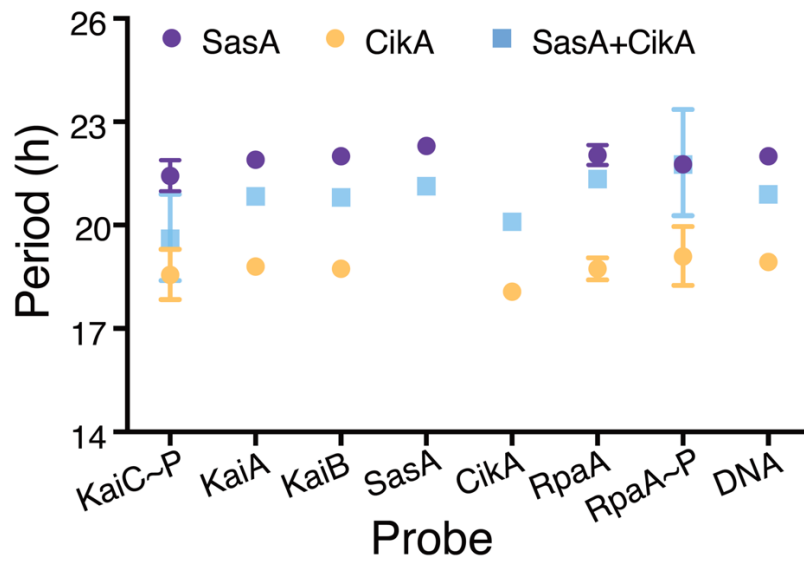


Figure S16. Counterbalancing effect of SasA and CikA on the period of the IVC.

Periods were calculated for each probe in IVC reactions containing SasA (purple), CikA (yellow) or both (blue). Each data point represents the mean from three independent measurements and vertical bars indicate the standard error. The SasA + CikA IVC produced the oscillations with a period of 20.9 ± 0.4 h. The SasA-only IVC showed a slight period lengthening, producing oscillations with a period of 21.9 ± 0.2 h, while the CikA-only IVC had a shorter period of 18.7 ± 0.3 h. These observations indicate that the period of clock is counterbalanced by the signal transduction proteins SasA and CikA.

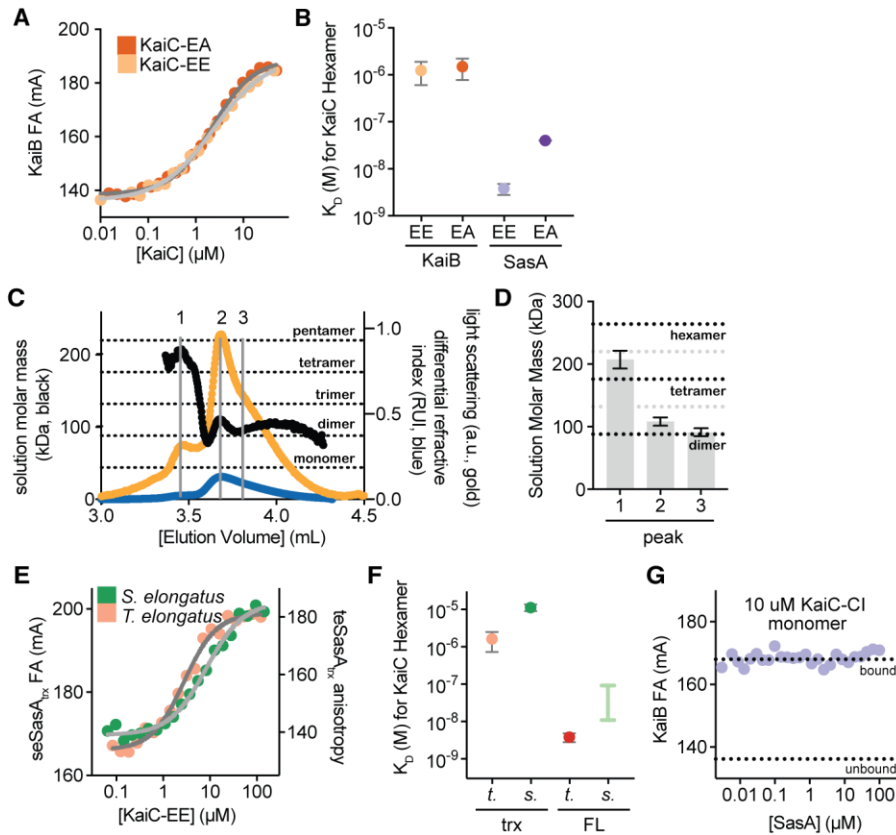


Figure S17. Biochemical properties of the SasA-KaiC interaction.

(A) KaiB binds to KaiC-EE and KaiC-EA with similar affinity. Representative equilibrium binding assays of 50 nM fluorescently labeled KaiB from *S. elongatus* in the presence of increasing concentrations of *S. elongatus* KaiC-EA (dark orange) and KaiC-EE (light orange). Data were fit to a Langmuir binding isotherm (EA, dark gray; EE, light gray). (B) SasA binds KaiC more tightly than does KaiB, with a preference for the pS/pT phosphomimetic, KaiC-EE. Calculated equilibrium dissociation constants (K_D) from binding data in panel A (mean \pm SD, $n = 3$; light and dark orange) are compared to affinities from Valencia et al. (50) (mean \pm SD, K_D measured by SPR; light and dark purple) for full-length SasA from *T. elongatus*. (C) Full-length SasA exists primarily a dimer in solution. Traces from a representative size-exclusion chromatography coupled to multiangle light scattering (SEC-MALS) run for full-length SasA from *S. elongatus*. Differential refractive index (blue) is depicted with light scattering (gold) and absolute mass estimation (kDa, black line). (D) Quantitative mass analysis of peaks indicated at the top of panel C (peaks 1-3) analyzed from triplicate SEC-MALS runs are consistent with a dimer-tetramer equilibrium (mean mass in kDa \pm SD). Calculated masses for dimer, tetramer and hexamer are represented by black dotted lines. (E) The SasA_{trx} domain of *T. elongatus* binds

with higher affinity than the *S. elongatus* SasA_{trx} domain to the respective KaiC-EE variant from each organism. Equilibrium binding assays of fluorescently labeled SasA_{trx} from *S. elongatus* (dark green) or *T. (pink) elongatus*. Data were fit as in panel **A**. **(F)** Full-length SasA (FL) binds much more tightly than the isolated SasA_{trx} domain (trx), suggesting that it relies on avidity for efficient binding to KaiC hexamer. Calculated K_D values extracted from data in panel **E** (mean \pm SD, n = 3; pink or dark green) are compared to affinities from Valencia et al. (31) (mean \pm SD, measured by SPR; red) for full-length SasA from *T. elongatus*. The affinity range of *S. elongatus* SasA calculated from the 2D titration data and our thermodynamic model (**Fig. 6**) is represented as a light green bar. **(G)** Full-length SasA does not display avidity and compete KaiB off of the KaiC-C1 monomer. Fluorescently labeled KaiB was bound to 10 μ M monomeric KaiC-C1 domain and subsequently titrated with full-length SasA as indicated. Anisotropy values for bound and unbound KaiB (dashed lines) were determined from curve fits in **Fig. S17A**.

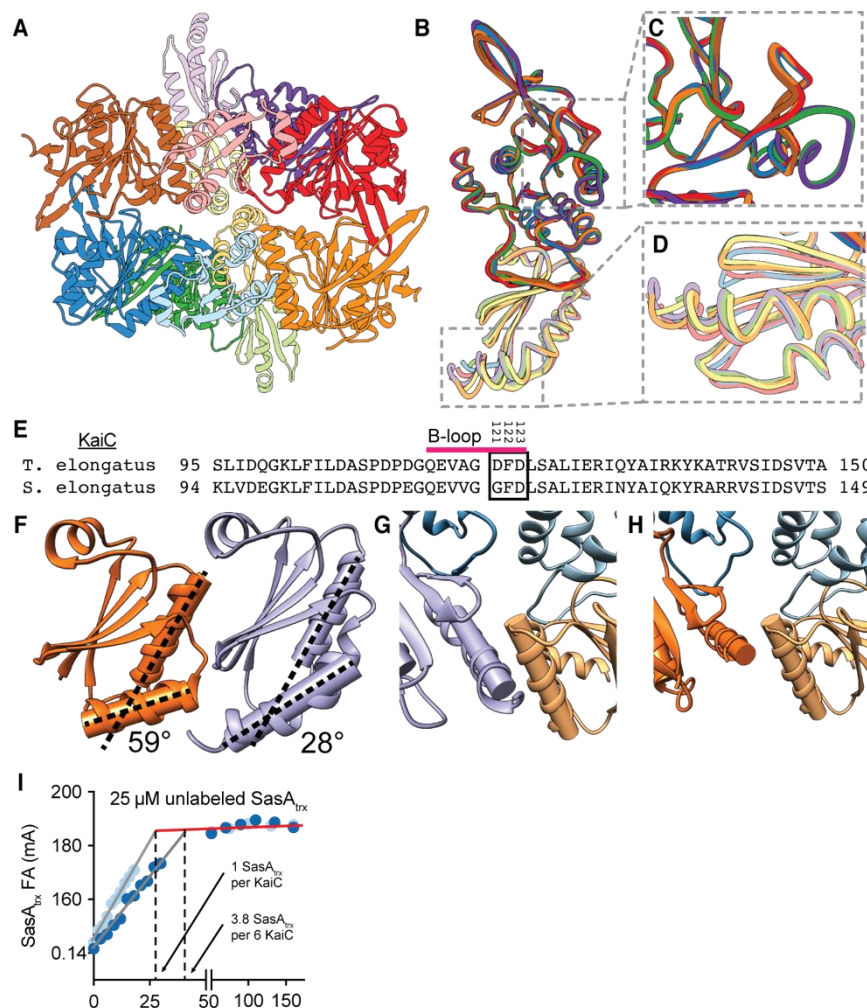


Figure S18. Structural details of the KaiC CI-SasA_{trx} complex.

(A) Asymmetric unit of the KaiC-CI-SasA_{trx} crystal complex (PDB 6X61). Individual KaiC-CI-SasA_{trx} pairs are depicted with SasA_{trx} subunits in light hues and KaiC-CI subunits in dark hues. (B-D) Modest structural heterogeneity was observed between the complexes of the asymmetric unit. Backbone overlays of the 6 KaiC CI-SasA_{trx} complexes from the asymmetric unit. Small differences are highlighted by the orientation of a loop comprising residues R185-V201 on the CI domain (panel C) or by the orientation of the α 3 helix of SasA_{trx} (panel D), with consensus among the complexes of chains CD and KL. (E) Sequence alignment of the B-loops (pink) and surrounding sequence from KaiC of *S. elongatus* and *T. elongatus*. Black box, residues at the shared KaiB and SasA-binding interface that were subjected to mutagenesis (F) SasA and fsKaiB diverge structurally at the α 3 helix. The α 1 and α 3 helices of fsKaiB (PDB: 5JWO) and SasA_{trx} (PDB: 6X61) are modeled as cylindrical axes with a radius of 1.8 Å, with the inter-axis crossing angle reported. (G-H) Orientation of the α 3 helix is likely to affect binding of KaiB at

the adjacent KaiC protomer. Helical orientation of the SasA_{trx} (purple, panel **G**) or fsKaiB (orange, panel **H**) domain relative to the α 1 helix on the adjacent KaiB molecule at the CW interface (yellow). Helices are represented as in panel **F**. **(I)** Representative saturation binding titrations of the *T. elongatus* KaiC-CI monomer or KaiC-EE hexamer in the presence of 25 μ M unlabeled SasA_{trx}. Stoichiometry of the saturated KaiC-SasA_{trx} complex was calculated at 3.8 ± 0.3 (mean \pm SD, n = 3) molecules of SasA per KaiC hexamer, consistent with measurements from native mass spectrometry (32). This calculation was made done by qualitatively separating the data into two linear regions and fitting each to a best fit line to describe the anisotropy after saturation (red line) and initial rate of anisotropy increase as a function of titrant concentration (gray line). The intersections of these lines (shown as dashed lines) represent the amount of KaiC needed to saturate the total SasA or KaiB concentration, which can be divided by the SasA concentration to give the KaiC to SasA ratio of the complex. We then assumed 1:1 binding between SasA and KaiC monomer to correct for errors in protein concentration and converted the ratio observed with hexamer to determine the number of SasA molecules per KaiC hexamer.

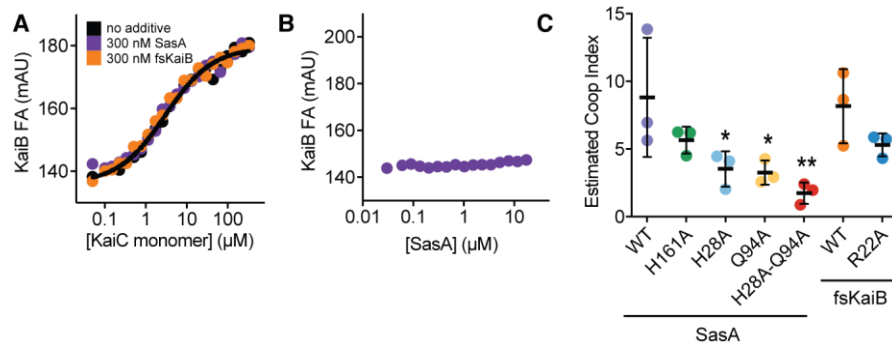
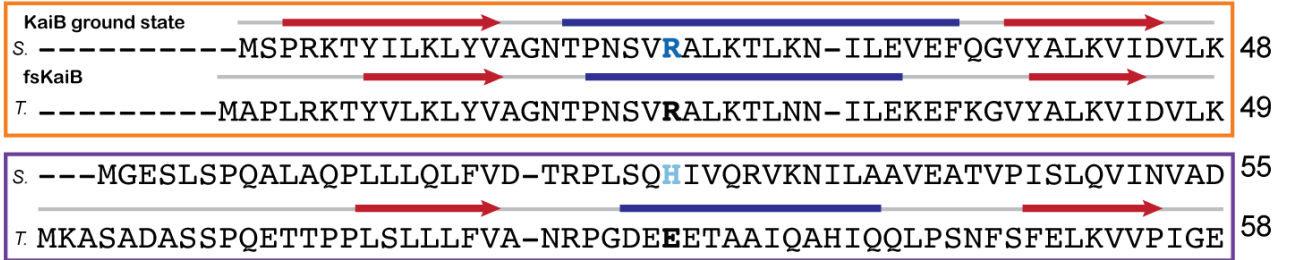


Figure S19. Validation of heterocooperative association model of KaiBC association.

(A) SasA and fsKaiB additives do not affect binding of 50 nM fluorescently labeled KaiB to KaiC-CI monomer. Equilibrium binding titration of fluorescently labeled KaiB with *S. elongatus* KaiC-CI monomer (black) in the presence of 300 nM fsKaiB (orange) or full-length SasA (purple). (B) KaiC is required for KaiB-SasA interactions. Equilibrium titration of fluorescently labeled KaiB with full-length SasA (purple), showing that KaiB anisotropy is unaffected without KaiC present. (C) Comparison of estimated cooperativity indices ($n = 3, \pm \text{SD}$) of various SasA and fsKaiB variants, as described in the main text (**Figure 7B**).

A non fold-switch region



fold-switch region

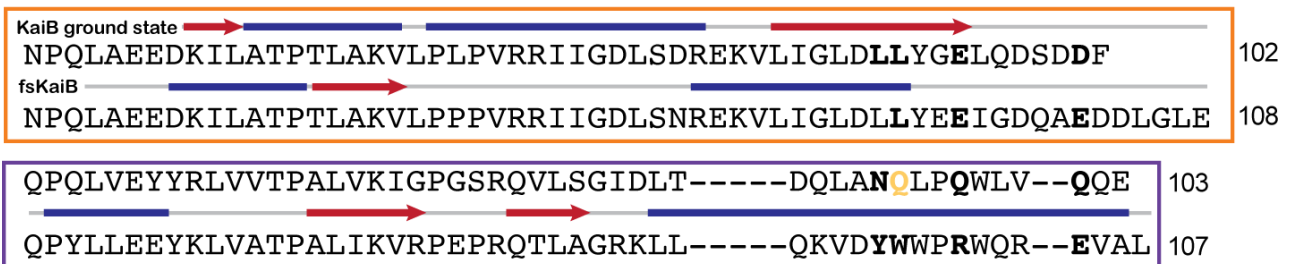


Figure S20. Multiple sequence alignment of KaiB and SasA_{trx} from *S.* and *T. elongatus*.

(A) Multiple sequence alignment of N-terminal (non-fold-switch) and C-terminal (fold-switch)

halves of KaiB (orange box) and the structurally analogous SasA_{trx} (purple box) from *S.*

elongatus and *T. elongatus*. Red arrows (β -sheets) and blue lines (α -helices) indicate secondary

structure from the KaiB tetramer (PDB: 2QKE), fsKaiB monomer (PDB: 5JWO) and SasA_{trx}

from the KaiC-CI-SasA_{trx} structure (PDB: 6X61) reported here. Mutations tested in this study are

depicted in bold.

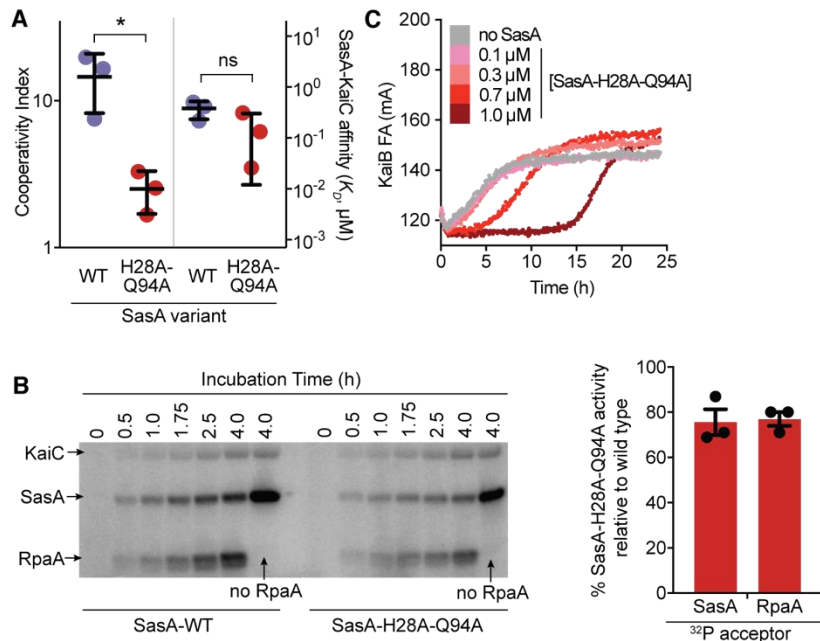


Figure S21. Biochemical characterization of various functions of the SasA-H28A-Q94A double mutant.

(A) Cooperativity index and KaiC affinity for wild-type SasA (purple dots) and SasA-H28A-Q94A double mutant (red dots) see Data S7. (B) Kinase assays were performed in the presence of γ - ^{32}P ATP as originally described in Takai et. al (19). These experiments were conducted with 5 μM KaiC-EE, 3.5 μM RpaA, and 2.5 μM SasA variant in 0.1 mM ATP. SasA-WT and SasA-H28A-Q94A were compared, tracking incorporation of ^{32}P into the proteins by SDS-PAGE and quantifying the result densitometrically. Slopes of the densitometry trajectories were compared in triplicate to estimate activity of the double mutant on RpaA as $77 \pm 5\%$ (mean \pm standard deviation). A no-RpaA control was included to quantify the efficiency of initial histidine phosphorylation in the SasA variants, and triplicate densitometries were compared at a single timepoint, with SasA-H28A-Q94A autophosphorylation $76 \pm 10\%$ as efficient as wild-type. (C) Representative trajectory of SasA-H28A-Q94A, titrated in the presence of 50 nM labeled KaiB probe as well as 3.5 μM KaiC and 1.2 μM KaiA (as shown for wild type in **Figure 4E**). SasA-H28A-Q94A were added here at a range of physiological and sub-physiological concentrations showing ~2-5 h delay in KaiB binding in presence of SasA-H28A-Q94A as compared to WT SasA.

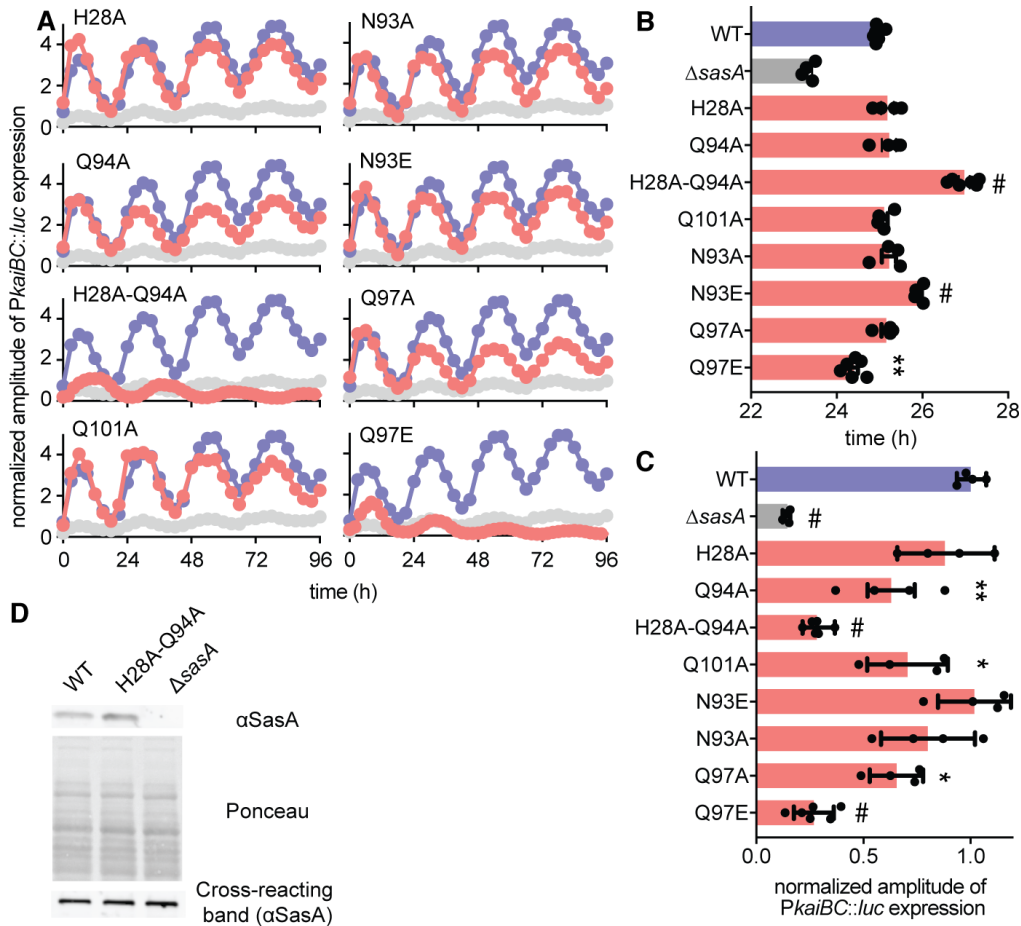


Figure S22. Mutations at the SasA-KaiB cooperativity interface alter circadian rhythms in *S. elongatus*.

(A) Bioluminescence traces produced by *S. elongatus* strains based on expression of firefly luciferase driven by the clock-controlled *kaiBC* promoter. Wild type (WT) and $\Delta sasA$ strains are compared to markerless CRISPR/Cas12a-edited *sasA* mutants, with the relevant amino acid substitutions indicated. Graphs display the averages of 6-12 wells, with standard deviation omitted for better visibility of multiple traces. WT (purple) and mutants, colored as in panel B. (B-C) Analysis of raw bioluminescence data was performed using BioDare2 to calculate the signal amplitude (in arbitrary units, a.u.) (panel B) and period length (panel C), with the average and standard deviation reported for 6-12 replicates. One-way ANOVA was performed to identify significant changes (*, $P < 0.05$; **, $P < 0.01$; #, $P < 0.0001$) in amplitude and period length relative to wild type. (D) Western blot showing similar expression levels of SasA at CT 24 in WT

and *sasA*-H28A-Q94A double mutant strains. The cross-reacting band shown at the bottom serves as loading control.

Table S1. Constructs and shorthand names used in this study.

Shorthand name	organism	Protein full name
KaiC	<i>S. elongatus</i>	FLAG-seKaiC-1-519
KaiC-AA		FLAG-seKaiC-1-519-S431A-T432A
KaiC-AE		FLAG-seKaiC-1-519-S431A-T432E
KaiC-EE		FLAG-seKaiC-1-519-S431E-T432E
KaiC-EA		FLAG-seKaiC-1-519-S431E-T432A
KaiC-CI monomer		FLAG-seKaiC-16-246-R40A-K172A
KaiC-EE	<i>T. elongatus</i>	FLAG-teKaiC-1-518-S431E-T432E
KaiC-EE-D121A		FLAG-teKaiC-1-518-D121A-S431E-T432E
KaiC-EE-F122A		FLAG-teKaiC-1-518-F122A-S431E-T432E
KaiC-EE-D123A		FLAG-teKaiC-1-518-D123A-S431E-T432E
KaiC-CI monomer		FLAG-teKaiC-17-247-R41A-K173A
KaiB	<i>S. elongatus</i>	seKaiB-1-102-FLAG
G-KaiB		Gly-seKaiB-1-102-FLAG
KaiB-K25C-6IAF		sekaiB-1-102-K25C-FLAG-6-iodoacetamido-fluorescein
fsKaiB		seKaiB-1-99-Y7A-I87A-Y93A-FLAG
fsKaiB-R22A		seKaiB-1-99-Y7A-R22A-I87A-Y93A-FLAG
KaiA		seKaiA-1-284
G-KaiA		Gly-seKaiA-1-284
SasA		seSasA-1-387
G-SasA		Gly-seSasA-1-387
G-SasA-H161A		Gly-seSasA-1-387-H161A
SasA		seSasA-1-387-FLAG
SasA-H161A		seSasA-1-387-H161A-FLAG
SasA-H28A		seSasA-1-387-H28A-FLAG
SasA-Q94A		seSasA-1-387-Q94A-FLAG
SasA-H28A-Q94A		seSasA-1-387-H28A-Q94A-FLAG
SasA _{trx} -Q31C*		FLAG-seSasA-13-103-P13A-FLAG
		FLAG-seSasA-13-103-P13A-Q31C-FLAG
SasA _{trx}		FLAG-teSasA-16-107-P16A-FLAG
SasA _{trx} -A35C*		FLAG-teSasA-16-107-P16A-A35C-FLAG
CikA		<i>S. elongatus</i>
CikA-LPTEGG-6IAF	FLAG-seCikA-1-754-LPET-GGGYC*(-6IAF)-N	
CikA-H393A	FLAG-seCikA-1-754-H393A	
CikA	FLAG-seCikA-1-754	
CikA _{psr}	seCikA-S605-606-745-C644S-C686S-C742S	
CikA _{psr} -S727C*	seCikA-S605-606-745-C644S-C686S-C742S-S727C	
RpaA	seRpaA-1-249	
GGG-RpaA	Gly ₃ -seRpaA-1-249	
RpaA-R121Q	seRpaA-1-249-R121Q	
G-RpaA-R121Q	Gly ₃ -seRpaA-1-249-R121Q	

* Single cysteine residue for labeling with 6-iodoacetamido-fluorescein

Table S2. Protein expression and purification conditions

Protein construct	Expression temperature and duration	Ni-NTA Loading buffer	Ni-NTA Wash buffer	Ni-NTA Elution buffer	Gel Filtration Column and Elution Buffer
G-KaiA	30 °C, 12 h	50 mM NaH ₂ PO ₄ , 500 mM NaCl, pH 8	50 mM NaH ₂ PO ₄ , 500 mM NaCl, 20 mM imidazole pH 8	50 mM NaH ₂ PO ₄ , 500 mM NaCl, 250 mM imidazole pH 8	Superdex-200-1660-pg 20 mM Tris, 150 mM NaCl, 5 mM MgCl ₂ , 1 mM ATP, pH 8
G-KaiB-FLAG	30 °C, 12 h	50 mM NaH ₂ PO ₄ , 500 mM NaCl, pH 8	50 mM NaH ₂ PO ₄ , 500 mM NaCl, 20 mM imidazole pH 8	50 mM NaH ₂ PO ₄ , 500 mM NaCl, 250 mM imidazole pH 8	Superdex-75-1660-pg 20 mM Tris, 150 mM NaCl, 5 mM MgCl ₂ , 1 mM ATP, pH 8
FLAG-KaiC	30 °C, 12 h	50 mM NaH ₂ PO ₄ , 500 mM NaCl, pH 8	50 mM NaH ₂ PO ₄ , 500 mM NaCl, 80 mM imidazole pH 8	50 mM NaH ₂ PO ₄ , 500 mM NaCl, 250 mM imidazole pH 8	Superdex-200-1660-pg 20 mM Tris, 150 mM NaCl, 5 mM MgCl ₂ , 1 mM ATP, pH 8
FLAG-KaiC-AA (S431A, T432A)	30 °C, 12 h	50 mM NaH ₂ PO ₄ , 500 mM NaCl, pH 8	50 mM NaH ₂ PO ₄ , 500 mM NaCl, 80 mM imidazole pH 8	50 mM NaH ₂ PO ₄ , 500 mM NaCl, 250 mM imidazole pH 8	Superdex-200-1660-pg 20 mM Tris, 150 mM NaCl, 5 mM MgCl ₂ , 1 mM ATP, pH 8
FLAG-KaiC-AE (S431A, T432E)	30 °C, 12 h	50 mM NaH ₂ PO ₄ , 500 mM NaCl, pH 8	50 mM NaH ₂ PO ₄ , 500 mM NaCl, 80 mM imidazole pH 8	50 mM NaH ₂ PO ₄ , 500 mM NaCl, 250 mM imidazole pH 8	Superdex-200-1660-pg 20 mM Tris, 150 mM NaCl, 5 mM MgCl ₂ , 1 mM ATP, pH 8
FLAG-KaiC-EE (S431E, T432E)	30 °C, 12 h	50 mM NaH ₂ PO ₄ , 500 mM NaCl, pH 8	50 mM NaH ₂ PO ₄ , 500 mM NaCl, 80 mM imidazole pH 8	50 mM NaH ₂ PO ₄ , 500 mM NaCl, 250 mM imidazole pH 8	Superdex-200-1660-pg 20 mM Tris, 150 mM NaCl, 5 mM MgCl ₂ , 1 mM ATP, pH 8
FLAG-KaiC-EA	30 °C, 12 h	50 mM NaH ₂ PO ₄ ,	50 mM NaH ₂ PO ₄ , 500 mM	50 mM NaH ₂ PO ₄ , 500 mM NaCl, 250	Superdex-200-1660-pg

(S431E, T432A)		500 mM NaCl, pH 8	NaCl, 80 mM imidazole pH 8	mM imidazole pH 8	20 mM Tris, 150 mM NaCl, 5 mM MgCl ₂ , 1 mM ATP, pH 8
G-SasA	30 °C, 12 h	50 mM NaH ₂ PO ₄ , 500 mM NaCl, pH 8	50 mM NaH ₂ PO ₄ , 500 mM NaCl, 20 mM imidazole pH 8	50 mM NaH ₂ PO ₄ , 500 mM NaCl, 250 mM imidazole pH 8 + 10 mM TCEP	Superdex-200-1660-pg 20 mM Tris, 150 mM NaCl, 5 mM MgCl ₂ , 1 mM ATP, pH 8
G-SasA-H161A	30 °C, 12 h	50 mM NaH ₂ PO ₄ , 500 mM NaCl, pH 8	50 mM NaH ₂ PO ₄ , 500 mM NaCl, 20 mM imidazole pH 8	50 mM NaH ₂ PO ₄ , 500 mM NaCl, 250 mM imidazole pH 8 + 10 mM TCEP	Superdex-200-1660-pg 20 mM Tris, 150 mM NaCl, 5 mM MgCl ₂ , 1 mM ATP, pH 8
FLAG-CikA-LPETGG	20 °C, 22 h	50 mM NaH ₂ PO ₄ , 500 mM NaCl, pH 8	50 mM NaH ₂ PO ₄ , 500 mM NaCl, 20 mM imidazole pH 8	50 mM NaH ₂ PO ₄ , 500 mM NaCl, 250 mM imidazole pH 8 + 20 mM TCEP	Superdex-200-1660-pg 20 mM Tris, 150 mM NaCl, 5 mM MgCl ₂ , pH 8
FLAG-CikA-H393A	20 °C, 22 h	50 mM NaH ₂ PO ₄ , 500 mM NaCl, pH 8	50 mM NaH ₂ PO ₄ , 500 mM NaCl, 20 mM imidazole pH 8	50 mM NaH ₂ PO ₄ , 500 mM NaCl, 250 mM imidazole pH 8 + 20 mM TCEP	Superdex-200-1660-pg 20 mM Tris, 150 mM NaCl, 5 mM MgCl ₂ , pH 8
GGG-RpaA	30 °C, 12 h	50 mM NaH ₂ PO ₄ , 500 mM NaCl, pH 8	50 mM NaH ₂ PO ₄ , 500 mM NaCl, 20 mM imidazole pH 8	50 mM NaH ₂ PO ₄ , 500 mM NaCl, 250 mM imidazole pH 8	Superdex-75-1660-pg 20 mM Tris, 150 mM NaCl, 5 mM MgCl ₂ , 1 mM ATP, pH 8
GGG-RpaA-R121Q	30 °C, 12 h	50 mM NaH ₂ PO ₄ , 500 mM NaCl, pH 8	50 mM NaH ₂ PO ₄ , 500 mM NaCl, 20 mM imidazole pH 8	50 mM NaH ₂ PO ₄ , 500 mM NaCl, 250 mM imidazole pH 8	Superdex-75-1660-pg 20 mM Tris, 150 mM NaCl, 5 mM MgCl ₂ , 1 mM ATP, pH 8

Table S3. Fluorophore labels and target proteins ligated using sortase-A

Target Protein	Label Position	Peptide with Fluorophore	Fluorophore Excitation Max (nm)	Fluorophore Emission Max (nm)
G-KaiA	N-terminal	C(Cy3)-LPETGG	554	568
G-KaiB-FLAG	N-terminal	5-FAM-LPETGG	480	520
G-SasA	N-terminal	5-FAM-LPETGG	480	520
GGG-RpaA	N-terminal	5-FAM-LPETGG	480	520
GGG-RpaA-R121Q	N-terminal	5-FAM-LPETGG	480	520
FLAG-CikA-LPETGG	C-terminal	GGGYC(6-IAF)-N	493	520
Fluorescently labeled synthetic DNA (Integrated DNA Technologies, Inc., Iowa, USA) (/4iCy3/ – internal labeling of DNA backbone with cyanoethyl phosphoramidite chemistry)				
<i>PkaiBC</i> 31-bp promoter sequence 5'-CCG/4iCy3/AGC TTA AGA CCT CCT TTA CCT TTT CAG G-3' 3'-GGC TCG AAT TCT GGA GGA AAT GGA AAA GTC C-5'			550	564

Initially, we labeled all the components with FAM. However, KaiA with N-terminal FAM produced noisy FA data. We empirically tested alternate fluorophores such as 6-IAF, Cy3, and Cy5, of which Cy3-labeled KaiA produced high quality FA data. For *PkaiBC* DNA, a FAM label conjugated to the 5'-end resulted in low signal-to-noise FA. In contrast, the Cy3-labeled *PkaiBC* produced high-quality FA data.

Table S4. In vitro clock reaction composition.

Component	Concentration
KaiA	1.20 μ M
KaiB-FLAG	3.50 μ M
FLAG-KaiC	3.50 μ M
SasA	0.65 μ M
FLAG-CikA	0.65 μ M
RpaA	2.50 μ M
<i>PkaiBC</i> , 31-bp promoter DNA	100 nM

Cellular concentrations of SasA, CikA, and RpaA as determined by semi-quantitative Western blotting were used to optimize concentrations of these proteins for IVC reactions (21). Optimal concentrations for the Kai proteins are well established (82).

Table S5. Specific reaction conditions with designated protein constructs.

Experiment Type	Protein Construct Shorthand Name / Final Concentration (μM if not indicated)	Experimental Condition
KaiA Titration Fluorescence Assay (Fig. 3A)	1) KaiB-K25C-6IAF / 0.05 2) KaiC / 3.5 3) KaiB / 3.45 4) KaiA / varied (0.3, 0.6, 1.2, 2.4, 3.6, 4.8, and 6.0)	<ul style="list-style-type: none"> • Volume: 80 μL • Buffer: 20 mM Tris, 150 mM NaCl, 5 mM MgCl_2, 1 mM ATP, 0.5 mM EDTA, pH 8.0 • Temperature: 30 $^\circ\text{C}$
KaiB Titration Fluorescence Assay (Fig. 3B)	1) KaiB-K25C-6IAF / 0.05 2) KaiC / 3.5 3) KaiB / varied (0.65, 0.825, 1.70, 3.45, 6.95, 10.45, and 17.45) 4) KaiA / 1.2	<ul style="list-style-type: none"> • Volume: 80 μL • Buffer: 20 mM Tris, 150 mM NaCl, 5 mM MgCl_2, 1 mM ATP, 0.5 mM EDTA, pH 8.0 • Temperature: 30 $^\circ\text{C}$
SasA Titration Fluorescence Assay under different KaiB concentrations (Fig. 4)	1) KaiB-K25C-6IAF / 0.05 2) KaiC / 3.5 3) KaiB / fixed at 0.825, 1.70, and 3.45 4) KaiA / 1.2 5) SasA / varied (0.0, 0.1, 0.65, 1.0, 1.8, 3.5, and 5.0)	<ul style="list-style-type: none"> • Volume: 80 μL • Buffer: 20 mM Tris, 150 mM NaCl, 5 mM MgCl_2, 1 mM ATP, 0.5 mM EDTA, pH 8.0 • Temperature: 30 $^\circ\text{C}$
CikA Titration Fluorescence Assay under different KaiA concentrations (Fig. 4)	1) KaiB-K25C-6IAF / 0.05 2) KaiC / 3.5 3) KaiB / 3.45 4) KaiA / fixed at 0.3 and 1.2 5) CikA / varied (0.0, 0.1, 0.65, 1.0, 1.8, 3.5, and 5.0)	<ul style="list-style-type: none"> • Volume: 80 μL • Buffer: 20 mM Tris, 150 mM NaCl, 5 mM MgCl_2, 1 mM ATP, 0.5 mM EDTA, pH 8.0 • Temperature: 30 $^\circ\text{C}$
SasA _{trx} Titration Fluorescence Assay under different KaiB concentrations (S15A)	1) KaiB-K25C-6IAF / 0.05 2) KaiC / 3.5 3) KaiB / fixed at 1.70 and 3.45 4) KaiA / 1.2 5) SasA _{trx} / varied (0.0, 0.1, 0.65, 1.0, 1.8, 3.5, and 5.0)	<ul style="list-style-type: none"> • Volume: 80 μL • Buffer: 20 mM Tris, 150 mM NaCl, 5 mM MgCl_2, 1 mM ATP, 0.5 mM EDTA, pH 8.0 • Temperature: 30 $^\circ\text{C}$
CikA _{psr} Titration Fluorescence Assay under different KaiA concentrations (S15B)	1) KaiB-K25C-6IAF / 0.05 2) KaiC / 3.5 3) KaiB / 3.45 4) KaiA / fixed at 0.3 and 1.2 5) CikA _{psr} / varied (0.0, 0.1, 0.65, 1.0, 1.8, 3.5, and 5.0)	<ul style="list-style-type: none"> • Volume: 80 μL • Buffer: 20 mM Tris, 150 mM NaCl, 5 mM MgCl_2, 1 mM ATP, 0.5 mM EDTA, pH 8.0 • Temperature: 30 $^\circ\text{C}$

Table S6. Refinement statistics for structure determination of KaiC-CI-SasAtrx complex.

Data collection	
Space group	P2 ₁
Cell dimensions	
<i>a</i> , <i>b</i> , <i>c</i> (Å)	107.6, 121.58, 133.59
α , β , γ (°)	90.0, 108.78, 90.0
Resolution (Å)	49.05-3.2 (3.30-3.20) *
No. of total reflections	153257 (13790)
No. Unique Reflections	53267 (4637)
<i>R</i> _{merge}	16.5 (75.7)
<i>R</i> _{pim}	13.0 (57.5)
I/ σ I	5.5 (1.5)
Completeness (%)	98.8 (99.3)
CC _{1/2}	0.95 (0.58)
Wilson B-factor	58.3
Redundancy	2.9 (3.0)
Refinement	
Resolution (Å)	3.20
<i>R</i> _{work} / <i>R</i> _{free}	22.2/26.6
No. atoms	
Protein	15469
Ligand/ion	30
B-factors	
Protein	61.3
Ligand/ion	46.1
R.m.s deviations	
Bond lengths (Å)	0.003
Bond angles (°)	0.78
Residues in favored regions (%)	93.1
Residues in outlier regions (%)	0.6

*Highest resolution shell is shown in parenthesis.

One crystal was used for data collection.

Data were collected at a wavelength of 1.0 Å.

Table S7. Period analysis, ordinary one-way ANOVA for fluorescence assays comparing different oscillator conditions.

Protein-concentration (μM) comparison with / altered protein-concentration	Mean Diff.	95.00% CI of diff.	Significant ?	Summary	Adjusted <i>P</i> Value
KaiB-3.5 / KaiB-1.75	-1.666	-3.238 to -0.09300	Yes	*	0.0354
KaiB-3.5 / KaiB-7.0	0.5423	-1.394 to 2.479	No	ns	0.8847
KaiB-3.5 / KaiB-10.5	0.5118	-1.561 to 2.584	No	ns	0.922
KaiB-3.5 / KaiB-17.5	1.244	-0.6920 to 3.181	No	ns	0.3047
SasA-0.0 / SasA-0.1	-0.498	-1.678 to 0.6824	No	ns	0.622
SasA-0.0 / SasA-0.3	-1.086	-2.266 to 0.09437	No	ns	0.0758
SasA-0.0 / SasA-0.65	-2.52	-3.700 to -1.340	Yes	***	0.0001
SasA-0.0 / SasA-1.0	-4.118	-5.298 to -2.938	Yes	#	<0.0001
SasA-0.0 / SasA-1.8	-12.76	-14.49 to -11.03	Yes	#	<0.0001
KaiB-1.75, SasA-0.0 / SasA-0.1	1.953	0.5292 to 3.377	Yes	**	0.0048
KaiB-1.75, SasA-0.0 / SasA-0.3	0.9688	-0.5609 to 2.498	No	ns	0.3415
KaiB-1.75, SasA-0.0 / SasA-0.65	-0.1362	-1.666 to 1.393	No	ns	0.9997
KaiB-1.75, SasA-0.0 / SasA-1.0	-1.861	-3.285 to -0.4367	Yes	**	0.0074
KaiB-1.75, SasA-0.0 / SasA-1.8	-8.009	-10.66 to -5.359	Yes	#	<0.0001
SasA _{trx} -0.0 / SasA _{trx} -0.1	-0.1257	-1.638 to 1.387	No	ns	0.9997
SasA _{trx} -0.0 / SasA _{trx} -0.3	-0.3682	-1.881 to 1.144	No	ns	0.9812
SasA _{trx} -0.0 / SasA _{trx} -0.65	-1.008	-2.521 to 0.5041	No	ns	0.3257
SasA _{trx} -0.0 / SasA _{trx} -1.0	-1.771	-3.283 to -0.2584	Yes	*	0.016
SasA _{trx} -0.0 / SasA _{trx} -1.8	-3.611	-5.123 to -2.098	Yes	#	<0.0001
SasA _{trx} -0.0 / SasA _{trx} -3.5	-7.318	-8.831 to -5.806	Yes	#	<0.0001
SasA _{trx} -0.0 / SasA _{trx} -5.0	-8.366	-10.03 to -6.701	Yes	#	<0.0001
KaiA-1.2 / KaiA-0.3	-5.433	-6.896 to -3.969	Yes	#	<0.0001
KaiA-1.2 / KaiA-0.6	-1.293	-2.833 to 0.2473	No	ns	0.1285
KaiA-1.2 / KaiA-2.4	0.5891	-0.9510 to 2.129	No	ns	0.8174
KaiA-1.2 / KaiA-3.6	0.9321	-0.7165 to 2.581	No	ns	0.4766
KaiA-1.2 / KaiA-4.8	-1.593	-3.702 to 0.5161	No	ns	0.2017
KaiA-1.2 / KaiA-6.0	-4.173	-6.985 to -1.361	Yes	**	0.002
CikA-0.0 / CikA-0.1	-0.04685	-0.1630 to 0.06934	No	ns	0.811
CikA-0.0 / CikA-0.3	-0.03718	-0.1534 to 0.07901	No	ns	0.9261
CikA-0.0 / CikA-0.65	-0.00668	-0.1229 to 0.1095	No	ns	0.9998
CikA-0.0 / CikA-1.0	0.04403	-0.07215 to 0.1602	No	ns	0.85
CikA-0.0 / CikA-1.8	0.1113	-0.004878 to 0.2275	No	ns	0.0654
CikA-0.0 / CikA-3.5	0.1006	-0.01555 to 0.2168	No	ns	0.1145
CikA-0.0 / CikA-5.0	0.1906	0.07439 to 0.3068	Yes	***	0.0004
KaiA-0.3, CikA-0.0 / CikA-0.1	0.75	-2.315 to 3.815	No	ns	0.9499
KaiA-0.3, CikA-0.0 / CikA-0.3	2.545	-0.5204 to 5.610	No	ns	0.1201
KaiA-0.3, CikA-0.0 / CikA-0.65	4.693	1.895 to 7.492	Yes	**	0.0014
KaiA-0.3, CikA-0.0 / CikA-1.0	5.02	2.222 to 7.818	Yes	***	0.0007

KaiA-0.3, CikA-0.0 / CikA-1.8	6.44	3.642 to 9.238	Yes	#	<0.0001
KaiA-0.3, CikA-0.0 / CikA-3.5	7.407	4.608 to 10.21	Yes	#	<0.0001
KaiA-0.3, CikA-0.0 / CikA-5.0	7.923	5.125 to 10.72	Yes	#	<0.0001
CikA _{psr} -0.0 / CikA _{psr} -0.1	3.01	2.132 to 3.889	Yes	#	<0.0001
CikA _{psr} -0.0 / CikA _{psr} -0.3	2.361	1.386 to 3.336	Yes	#	<0.0001
CikA _{psr} -0.0 / CikA _{psr} -0.65	1.658	0.7792 to 2.536	Yes	#	<0.0001
CikA _{psr} -0.0 / CikA _{psr} -1.0	0.8853	0.006697 to 1.764	Yes	*	0.0476
CikA _{psr} -0.0 / CikA _{psr} -1.8	0.6953	-0.1833 to 1.574	No	ns	0.1771
CikA _{psr} -0.0 / CikA _{psr} -3.5	0.5711	-0.4036 to 1.546	No	ns	0.4758
CikA _{psr} -0.0 / CikA _{psr} -5.0	-0.1997	-1.078 to 0.6789	No	ns	0.9893
KaiB-1.75, SasA _{trx} -0.0 / SasA _{trx} -0.1	2.256	-1.984 to 6.496	No	ns	0.4607
KaiB-1.75, SasA _{trx} -0.0 / SasA _{trx} -0.3	1.906	-2.334 to 6.146	No	ns	0.6179
KaiB-1.75, SasA _{trx} -0.0 / SasA _{trx} -0.65	1.131	-3.109 to 5.371	No	ns	0.9285
KaiB-1.75, SasA _{trx} -0.0 / SasA _{trx} -1.0	0.416	-3.824 to 4.656	No	ns	0.9996
KaiB-1.75, SasA _{trx} -0.0 / SasA _{trx} -1.8	-3.684	-7.924 to 0.5561	No	ns	0.0974
KaiB-1.75, SasA _{trx} -0.0 / SasA _{trx} -3.5	-11.24	-15.48 to -6.999	Yes	#	<0.0001
KaiA-0.3, CikA _{psr} -0.0 / CikA _{psr} -0.1	-0.065	-6.407 to 6.277	No	ns	>0.9999
KaiA-0.3, CikA _{psr} -0.0 / CikA _{psr} -0.3	0.505	-5.837 to 6.847	No	ns	0.9997
KaiA-0.3, CikA _{psr} -0.0 / CikA _{psr} -0.65	1.13	-5.212 to 7.472	No	ns	0.9937
KaiA-0.3, CikA _{psr} -0.0 / CikA _{psr} -1.0	1.905	-4.437 to 8.247	No	ns	0.9136
KaiA-0.3, CikA _{psr} -0.0 / CikA _{psr} -1.8	2.21	-4.132 to 8.552	No	ns	0.845
KaiA-0.3, CikA _{psr} -0.0 / CikA _{psr} -3.5	4.11	-2.232 to 10.45	No	ns	0.3006
KaiA-0.3, CikA _{psr} -0.0 / CikA _{psr} -5.0	4.47	-1.872 to 10.81	No	ns	0.2302

Ordinary one-way ANOVA performed with Dunnett's multiple comparisons test was used to compare period values under specified conditions: ns, not significant; *, $P < 0.05$; **, $P < 0.01$; ***, $P < 0.001$; #, $P < 0.0001$. If not specified, fluorescence assays were run with 1.2 μM KaiA, 3.45 μM KaiB, 3.5 μM KaiC, and 0.05 μM fluorescently labeled KaiB probe.

Table S8. Amplitude analysis, ordinary one-way ANOVA for fluorescence assays comparing different oscillator conditions.

Protein-concentration (μM) comparison with / altered protein-concentration	Mean Diff.	95.00% CI of diff.	Significant?	Summary	Adjusted <i>P</i> Value
KaiB-3.5 / KaiB-1.75	0.08743	-0.02121 to 0.1961	No	ns	0.1437
KaiB-3.5 / KaiB-7.0	0.04213	-0.07417 to 0.1584	No	ns	0.7636
KaiB-3.5 / KaiB-10.5	0.04656	-0.06209 to 0.1552	No	ns	0.6484
KaiB-3.5 / KaiB-17.5	0.434	0.3457 to 0.5222	Yes	#	<0.0001
SasA-0.0 / SasA-0.1	-0.03844	-0.1930 to 0.1162	No	ns	0.9098
SasA-0.0 / SasA-0.3	0.02229	-0.1323 to 0.1769	No	ns	0.989
SasA-0.0 / SasA-0.65	0.1149	-0.03974 to 0.2694	No	ns	0.1799
SasA-0.0 / SasA-1.0	0.2204	0.06584 to 0.3750	Yes	**	0.0047
SasA-0.0 / SasA-1.8	0.4423	0.2160 to 0.6686	Yes	***	0.0003
KaiB-1.75, SasA-0.0 / SasA-0.1	-0.4206	-0.6723 to -0.1688	Yes	***	0.0007
KaiB-1.75, SasA-0.0 / SasA-0.3	-0.5336	-0.8040 to -0.2632	Yes	#	<0.0001
KaiB-1.75, SasA-0.0 / SasA-0.65	-0.524	-0.7944 to -0.2535	Yes	***	0.0001
KaiB-1.75, SasA-0.0 / SasA-1.0	-0.3502	-0.6019 to -0.09843	Yes	**	0.0043
KaiB-1.75, SasA-0.0 / SasA-1.8	0.007592	-0.4608 to 0.4759	No	ns	>0.9999
SasA _{trx} -0.0 / SasA _{trx} -0.1	-0.04557	-0.1360 to 0.04490	No	ns	0.6219
SasA _{trx} -0.0 / SasA _{trx} -0.3	-0.03403	-0.1245 to 0.05644	No	ns	0.8555
SasA _{trx} -0.0 / SasA _{trx} -0.65	0.06425	-0.02622 to 0.1547	No	ns	0.2642
SasA _{trx} -0.0 / SasA _{trx} -1.0	0.1418	0.05135 to 0.2323	Yes	***	0.0009
SasA _{trx} -0.0 / SasA _{trx} -1.8	0.2437	0.1532 to 0.3341	Yes	#	<0.0001
SasA _{trx} -0.0 / SasA _{trx} -3.5	0.3859	0.2954 to 0.4763	Yes	#	<0.0001
SasA _{trx} -0.0 / SasA _{trx} -5.0	0.4243	0.3247 to 0.5239	Yes	#	<0.0001
KaiA-1.2 / KaiA-0.3	0.3983	0.1870 to 0.6096	Yes	***	0.0001
KaiA-1.2 / KaiA-0.6	0.1897	-0.02157 to 0.4010	No	ns	0.0919
KaiA-1.2 / KaiA-2.4	0.12	-0.09133 to 0.3313	No	ns	0.4707
KaiA-1.2 / KaiA-3.6	0.2376	0.01147 to 0.4638	Yes	*	0.0365
KaiA-1.2 / KaiA-4.8	0.4218	0.1324 to 0.7111	Yes	**	0.0025
KaiA-1.2 / KaiA-6.0	0.4745	0.08869 to 0.8602	Yes	*	0.0115
CikA-0.0 / CikA-0.1	-0.04685	-0.1630 to 0.06934	No	ns	0.811
CikA-0.0 / CikA-0.3	-0.03718	-0.1534 to 0.07901	No	ns	0.9261
CikA-0.0 / CikA-0.65	-0.00668	-0.1229 to 0.1095	No	ns	0.9998
CikA-0.0 / CikA-1.0	0.04403	-0.07215 to 0.1602	No	ns	0.85
CikA-0.0 / CikA-1.8	0.1113	-0.004878 to 0.2275	No	ns	0.0654
CikA-0.0 / CikA-3.5	0.1006	-0.01555 to 0.2168	No	ns	0.1145
CikA-0.0 / CikA-5.0	0.1906	0.07439 to 0.3068	Yes	***	0.0004
KaiA-0.3, CikA-0.0 / CikA-0.1	-0.09828	-0.3229 to 0.1263	No	ns	0.7137
KaiA-0.3, CikA-0.0 / CikA-0.3	-0.1326	-0.3571 to 0.09201	No	ns	0.4194
KaiA-0.3, CikA-0.0 / CikA-0.65	-0.05589	-0.2519 to 0.1401	No	ns	0.9446

KaiA-0.3, CikA-0.0 / CikA-1.0	-0.1135	-0.3095 to 0.08252	No	ns	0.4393
KaiA-0.3, CikA-0.0 / CikA-1.8	-0.1124	-0.3085 to 0.08358	No	ns	0.449
KaiA-0.3, CikA-0.0 / CikA-3.5	-0.1599	-0.3560 to 0.03607	No	ns	0.1412
KaiA-0.3, CikA-0.0 / CikA-5.0	-0.1116	-0.3076 to 0.08441	No	ns	0.4568
CikA _{psr} -0.0 / CikA _{psr} -0.1	0.01182	-0.2952 to 0.3189	No	ns	0.9999
CikA _{psr} -0.0 / CikA _{psr} -0.3	-0.0595	-0.3976 to 0.2786	No	ns	0.9971
CikA _{psr} -0.0 / CikA _{psr} -0.65	0.02002	-0.2870 to 0.3271	No	ns	0.9997
CikA _{psr} -0.0 / CikA _{psr} -1.0	0.06736	-0.2397 to 0.3744	No	ns	0.9899
CikA _{psr} -0.0 / CikA _{psr} -1.8	0.08699	-0.2201 to 0.3941	No	ns	0.9588
CikA _{psr} -0.0 / CikA _{psr} -3.5	0.196	-0.1420 to 0.5341	No	ns	0.4727
CikA _{psr} -0.0 / CikA _{psr} -5.0	0.1054	-0.2016 to 0.4125	No	ns	0.9001
KaiB-1.75, SasA _{trx} -0.0 / SasA _{trx} -0.1	-0.05691	-0.4526 to 0.3388	No	ns	0.9957
KaiB-1.75, SasA _{trx} -0.0 / SasA _{trx} -0.3	-0.2672	-0.6629 to 0.1285	No	ns	0.2498
KaiB-1.75, SasA _{trx} -0.0 / SasA _{trx} -0.65	-0.3274	-0.7231 to 0.06834	No	ns	0.1199
KaiB-1.75, SasA _{trx} -0.0 / SasA _{trx} -1.0	-0.1683	-0.5640 to 0.2275	No	ns	0.6662
KaiB-1.75, SasA _{trx} -0.0 / SasA _{trx} -1.8	-0.08904	-0.4848 to 0.3067	No	ns	0.9653
KaiB-1.75, SasA _{trx} -0.0 / SasA _{trx} -3.5	-0.06065	-0.4564 to 0.3351	No	ns	0.9946
KaiA-0.3, CikA _{psr} -0.0 / CikA _{psr} -0.1	-0.06478	-0.3795 to 0.2500	No	ns	0.9863
KaiA-0.3, CikA _{psr} -0.0 / CikA _{psr} -0.3	-0.06702	-0.3818 to 0.2477	No	ns	0.9833
KaiA-0.3, CikA _{psr} -0.0 / CikA _{psr} -0.65	-0.1085	-0.4233 to 0.2063	No	ns	0.851
KaiA-0.3, CikA _{psr} -0.0 / CikA _{psr} -1.0	-0.09977	-0.4145 to 0.2150	No	ns	0.892
KaiA-0.3, CikA _{psr} -0.0 / CikA _{psr} -1.8	-0.05927	-0.3740 to 0.2555	No	ns	0.9918
KaiA-0.3, CikA _{psr} -0.0 / CikA _{psr} -3.5	-0.134	-0.4487 to 0.1808	No	ns	0.7026
KaiA-0.3, CikA _{psr} -0.0 / CikA _{psr} -5.0	-0.1477	-0.4625 to 0.1670	No	ns	0.6145

Ordinary one-way ANOVA performed with Dunnett's multiple comparisons test was used to compare amplitude values under specified conditions: ns, not significant; *, $P < 0.05$; **, $P < 0.01$; ***, $P < 0.001$; #, $P < 0.0001$. If not specified, fluorescence assays were run with 1.2 μM KaiA, 3.45 μM KaiB, 3.5 μM KaiC, and 0.05 μM fluorescently labeled KaiB probe.

Table S9. Ordinary two-way ANOVA of period values from fluorescence assays with pairwise comparisons showing how core oscillator components modulate SasA or Cika effects.

[Fixed protein-concentration] protein-concentration comparison with / altered protein-concentration (μ M)	Predicted (LS) mean diff.	95.00% CI of diff.	Significant ?	Summary	Adjusted P Value	N1	N2
[SasA-0.0] KaiB-3.5 / KaiB-1.75	-1.666	-2.798 to -0.5337	Yes	**	0.0021	7	12
[SasA-0.0] KaiB-3.5 / KaiB-7.0	0.5423	-0.8515 to 1.936	No	ns	0.6753	7	5
[SasA-0.0] KaiB-3.5 / KaiB-17.5	1.244	-0.1495 to 2.638	No	ns	0.0907	7	5
[SasA-0.1] KaiB-3.5 / KaiB-1.75	0.02	-1.493 to 1.533	No	ns	>0.9999	5	5
[SasA-0.1] KaiB-3.5 / KaiB-7.0	0.808	-0.9387 to 2.555	No	ns	0.5642	5	3
[SasA-0.1] KaiB-3.5 / KaiB-17.5	1.228	-0.5187 to 2.975	No	ns	0.2316	5	3
[SasA-0.3] KaiB-3.5 / KaiB-1.75	-0.3765	-1.983 to 1.230	No	ns	0.9059	5	4
[SasA-0.3] KaiB-3.5 / KaiB-7.0	0.826	-0.9225 to 2.575	No	ns	0.5504	5	3
[SasA-0.3] KaiB-3.5 / KaiB-17.5	1.069	-0.6792 to 2.818	No	ns	0.3404	5	3
[SasA-0.65] KaiB-3.5 / KaiB-1.75	-0.0475	-1.654 to 1.559	No	ns	0.9997	5	4
[SasA-0.65] KaiB-3.5 / KaiB-7.0	0.56	-1.189 to 2.309	No	ns	0.7967	5	3
[SasA-0.65] KaiB-3.5 / KaiB-17.5	1.103	-0.6452 to 2.852	No	ns	0.3152	5	3
[SasA-1.0] KaiB-3.5 / KaiB-1.75	-0.174	-1.687 to 1.339	No	ns	0.9868	5	5
[SasA-1.0] KaiB-3.5 / KaiB-7.0	1.041	-0.7054 to 2.788	No	ns	0.3594	5	3
[SasA-1.0] KaiB-3.5 / KaiB-17.5	0.8813	-0.8654 to 2.628	No	ns	0.4959	5	3
[SasA-1.8] KaiB-3.5 / KaiB-1.75	2	-0.2738 to 4.274	No	ns	0.0925	2	2
[SasA-1.8] KaiB-3.5 / KaiB-7.0	3.375	0.5902 to 6.160	Yes	*	0.0149	2	1
[Cika-0.0] KaiA-1.2 / KaiA-0.3	-5.433	-6.313 to -4.552	Yes	#	<0.0001	7	6
[Cika-0.0] KaiA-1.2 / KaiA-0.6	-1.293	-2.220 to -0.3661	Yes	**	0.0031	7	5
[Cika-0.0] KaiA-1.2 / KaiA-2.4	0.5891	-0.3376 to 1.516	No	ns	0.3347	7	5
[Cika-0.0] KaiA-1.2 / KaiA-3.6	0.9321	-0.05985 to 1.924	No	ns	0.0719	7	4
[Cika-0.1] KaiA-1.2 / KaiA-0.3	-4.394	-5.728 to -3.060	Yes	#	<0.0001	5	2
[Cika-0.1] KaiA-1.2 / KaiA-0.6	-1.441	-2.605 to -0.2764	Yes	**	0.0098	5	3
[Cika-0.1] KaiA-1.2 / KaiA-2.4	0.4493	-0.7150 to 1.614	No	ns	0.7689	5	3
[Cika-0.1] KaiA-1.2 / KaiA-3.6	-0.174	-1.920 to 1.572	No	ns	0.9979	5	1
[Cika-0.3] KaiA-1.2 / KaiA-0.3	-2.871	-4.205 to -1.537	Yes	#	<0.0001	5	2
[Cika-0.3] KaiA-1.2 / KaiA-0.6	-1.113	-2.277 to 0.05163	No	ns	0.0659	5	3
[Cika-0.3] KaiA-1.2 / KaiA-2.4	0.3707	-0.7936 to 1.535	No	ns	0.8669	5	3
[Cika-0.3] KaiA-1.2 / KaiA-3.6	0.274	-1.472 to 2.020	No	ns	0.9885	5	1
[Cika-0.65] KaiA-1.2 / KaiA-0.3	-1.215	-2.209 to -0.2202	Yes	*	0.012	5	3
[Cika-0.65] KaiA-1.2 / KaiA-0.6	-0.908	-1.902 to 0.08644	No	ns	0.0824	5	3
[Cika-0.65] KaiA-1.2 / KaiA-2.4	0.222	-0.7724 to 1.216	No	ns	0.9194	5	3
[Cika-1.0] KaiA-1.2 / KaiA-0.3	-1.308	-2.302 to -0.3136	Yes	**	0.0061	5	3
[Cika-1.0] KaiA-1.2 / KaiA-0.6	-0.5813	-1.576 to 0.4131	No	ns	0.3817	5	3
[Cika-1.0] KaiA-1.2 / KaiA-2.4	0.05533	-0.9391 to 1.050	No	ns	0.9985	5	3
[Cika-1.8] KaiA-1.2 / KaiA-0.3	-0.55	-1.713 to 0.6129	No	ns	0.6158	5	3

[CikA-1.8] KaiA-1.2 / KaiA-0.6	-0.87	-2.033 to 0.2929	No	ns	0.2068	5	3
[CikA-1.8] KaiA-1.2 / KaiA-2.4	-0.04667	-1.210 to 1.116	No	ns	0.9999	5	3
[CikA-1.8] KaiA-1.2 / KaiA-3.6	-1.51	-3.254 to 0.2344	No	ns	0.1114	5	1
[CikA-3.5] KaiA-1.2 / KaiA-0.3	0.1247	-0.8698 to 1.119	No	ns	0.9839	5	3
[CikA-3.5] KaiA-1.2 / KaiA-0.6	-0.1687	-1.163 to 0.8258	No	ns	0.962	5	3
[CikA-3.5] KaiA-1.2 / KaiA-2.4	0.3213	-0.6731 to 1.316	No	ns	0.7969	5	3
[CikA-5.0] KaiA-1.2 / KaiA-0.3	0.1613	-1.002 to 1.324	No	ns	0.9926	5	3
[CikA-5.0] KaiA-1.2 / KaiA-0.6	-0.1953	-1.358 to 0.9676	No	ns	0.9847	5	3
[CikA-5.0] KaiA-1.2 / KaiA-2.4	-0.132	-1.295 to 1.031	No	ns	0.9965	5	3
[CikA-5.0] KaiA-1.2 / KaiA-3.6	-4.302	-6.046 to -2.558	Yes	#	<0.0001	5	1

Ordinary two-way ANOVA performed with Dunnett's multiple comparisons test was used to compare pairwise period values under specified conditions: ns, not significant; *, $P < 0.05$; **, $P < 0.01$; ***, $P < 0.001$; #, $P < 0.0001$. Predicted least squared (LS) mean difference is reported instead of mean due to comparing means with different number of independent experiments. N1 and N2 specify the number of independent experiments that were able to be fit by FFT-NLLS with the online BioDare suite for the first and second conditions being compared, respectively (60, 61). If not specified, oscillators were run with 1.2 μM KaiA, 3.45 μM KaiB, 3.5 μM KaiC, and 0.05 μM fluorescently labeled KaiB probe.

Table S10. Ordinary two-way ANOVA of amplitude values from fluorescence assays with pairwise comparisons showing how core oscillator components modulate SasA or CikA effects.

[Fixed protein-concentration] protein-concentration comparison with / altered protein-concentration (μ M)	Predicted (LS) mean diff.	95.00% CI of diff.	Significant ?	Summary	Adjusted P Value	N1	N2
[SasA-0.0] KaiB-3.5 / KaiB-1.75	0.434	0.3145 to 0.5535	Yes	#	<0.0001	7	12
[SasA-0.0] KaiB-3.5 / KaiB-7.0	0.04656	-0.1006 to 0.1937	No	ns	0.7909	7	5
[SasA-0.0] KaiB-3.5 / KaiB-17.5	0.08743	-0.05971 to 0.2346	No	ns	0.3543	7	5
[SasA-0.1] KaiB-3.5 / KaiB-1.75	0.04169	-0.1180 to 0.2014	No	ns	0.8745	5	5
[SasA-0.1] KaiB-3.5 / KaiB-7.0	0.06957	-0.1148 to 0.2540	No	ns	0.7056	5	3
[SasA-0.1] KaiB-3.5 / KaiB-17.5	0.1301	-0.05432 to 0.3145	No	ns	0.2293	5	3
[SasA-0.3] KaiB-3.5 / KaiB-1.75	-0.1321	-0.3016 to 0.03751	No	ns	0.164	5	4
[SasA-0.3] KaiB-3.5 / KaiB-7.0	0.04368	-0.1409 to 0.2283	No	ns	0.9036	5	3
[SasA-0.3] KaiB-3.5 / KaiB-17.5	0.07517	-0.1094 to 0.2598	No	ns	0.6589	5	3
[SasA-0.65] KaiB-3.5 / KaiB-1.75	-0.215	-0.3845 to -0.04541	Yes	**	0.0089	5	4
[SasA-0.65] KaiB-3.5 / KaiB-7.0	-0.05956	-0.2442 to 0.1250	No	ns	0.7932	5	3
[SasA-0.65] KaiB-3.5 / KaiB-17.5	0.01352	-0.1711 to 0.1981	No	ns	0.9966	5	3
[SasA-1.0] KaiB-3.5 / KaiB-1.75	-0.1468	-0.3065 to 0.01293	No	ns	0.0792	5	5
[SasA-1.0] KaiB-3.5 / KaiB-7.0	0.04559	-0.1388 to 0.2300	No	ns	0.8907	5	3
[SasA-1.0] KaiB-3.5 / KaiB-17.5	0.03213	-0.1523 to 0.2165	No	ns	0.9571	5	3
[SasA-1.8] KaiB-3.5 / KaiB-1.75	0.01854	-0.2246 to 0.2617	No	ns	0.9792	2	2
[SasA-1.8] KaiB-3.5 / KaiB-7.0	-0.01082	-0.3086 to 0.2869	No	ns	0.9952	2	1
[CikA-0.0] KaiA-1.2 / KaiA-0.3	0.3983	0.2520 to 0.5447	Yes	#	<0.0001	7	5
[CikA-0.0] KaiA-1.2 / KaiA-0.6	0.1897	0.04336 to 0.3361	Yes	**	0.0066	7	5
[CikA-0.0] KaiA-1.2 / KaiA-2.4	0.12	-0.02640 to 0.2663	No	ns	0.1407	7	5
[CikA-0.0] KaiA-1.2 / KaiA-3.6	0.2376	0.08098 to 0.3943	Yes	**	0.0012	7	4
[CikA-0.1] KaiA-1.2 / KaiA-0.3	0.3469	0.1364 to 0.5574	Yes	***	0.0004	5	2
[CikA-0.1] KaiA-1.2 / KaiA-0.6	0.1197	-0.06407 to 0.3034	No	ns	0.325	5	3
[CikA-0.1] KaiA-1.2 / KaiA-2.4	0.0546	-0.1291 to 0.2383	No	ns	0.8923	5	3
[CikA-0.1] KaiA-1.2 / KaiA-3.6	0.2974	0.02178 to 0.5730	Yes	*	0.0299	5	1
[CikA-0.3] KaiA-1.2 / KaiA-0.3	0.3029	0.09246 to 0.5134	Yes	**	0.0021	5	2
[CikA-0.3] KaiA-1.2 / KaiA-0.6	0.08615	-0.09757 to 0.2699	No	ns	0.626	5	3
[CikA-0.3] KaiA-1.2 / KaiA-2.4	0.06877	-0.1150 to 0.2525	No	ns	0.7871	5	3
[CikA-0.3] KaiA-1.2 / KaiA-3.6	0.4703	0.1947 to 0.7459	Yes	***	0.0002	5	1
[CikA-0.65] KaiA-1.2 / KaiA-0.3	0.3491	0.1872 to 0.5111	Yes	#	<0.0001	5	3
[CikA-0.65] KaiA-1.2 / KaiA-0.6	0.06287	-0.09909 to 0.2248	No	ns	0.6955	5	3
[CikA-0.65] KaiA-1.2 / KaiA-2.4	0.08232	-0.07964 to 0.2443	No	ns	0.4976	5	3
[CikA-1.0] KaiA-1.2 / KaiA-0.3	0.2408	0.07883 to 0.4027	Yes	**	0.0017	5	3
[CikA-1.0] KaiA-1.2 / KaiA-0.6	0.06642	-0.09553 to 0.2284	No	ns	0.6594	5	3
[CikA-1.0] KaiA-1.2 / KaiA-2.4	0.0411	-0.1209 to 0.2031	No	ns	0.8874	5	3
[CikA-1.8] KaiA-1.2 / KaiA-0.3	0.1746	-0.008936 to 0.3581	No	ns	0.0675	5	3

[CikA-1.8] KaiA-1.2 / KaiA-0.6	-0.03042	-0.2139 to 0.1531	No	ns	0.9854	5	3
[CikA-1.8] KaiA-1.2 / KaiA-2.4	0.08793	-0.09558 to 0.2714	No	ns	0.6045	5	3
[CikA-1.8] KaiA-1.2 / KaiA-3.6	0.262	-0.01327 to 0.5373	No	ns	0.0673	5	1
[CikA-3.5] KaiA-1.2 / KaiA-0.3	0.1377	-0.02421 to 0.2997	No	ns	0.1154	5	3
[CikA-3.5] KaiA-1.2 / KaiA-0.6	-0.03605	-0.1980 to 0.1259	No	ns	0.92	5	3
[CikA-3.5] KaiA-1.2 / KaiA-2.4	0.1386	-0.02338 to 0.3005	No	ns	0.1124	5	3
[CikA-5.0] KaiA-1.2 / KaiA-0.3	0.09614	-0.08737 to 0.2796	No	ns	0.5253	5	3
[CikA-5.0] KaiA-1.2 / KaiA-0.6	-0.02335	-0.2069 to 0.1602	No	ns	0.9947	5	3
[CikA-5.0] KaiA-1.2 / KaiA-2.4	0.07869	-0.1048 to 0.2622	No	ns	0.6934	5	3
[CikA-5.0] KaiA-1.2 / KaiA-3.6	0.2078	-0.06747 to 0.4830	No	ns	0.1999	5	1

Ordinary two-way ANOVA performed with Dunnett's multiple comparisons test was used to compare pairwise amplitude values under specified conditions: ns, not significant; *, $P < 0.05$; **, $P < 0.01$; ***, $P < 0.001$; #, $P < 0.0001$. Predicted least squared (LS) mean difference is reported instead of mean due to comparing means with different number of independent experiments. N1 and N2 specify the number of independent experiments that were able to be fit by FFT-NLLS with the online BioDare suite for the first and second conditions being compared, respectively (60, 61). If not specified, oscillators were run with 1.2 μM KaiA, 3.45 μM KaiB, 3.5 μM KaiC, and 0.05 μM fluorescently labeled KaiB probe.

Table S11. Cyanobacterial strains used in this study.

Strain	Genotype (NS denotes neutral site)	Antibiotic resistance	Source
WT (AMC541)	NSII-P _{kaiBC} :: <i>luc</i>	Cm	Lab collection
Δ <i>sasA</i> (AMC1192)	NSII-P _{kaiBC} :: <i>luc</i> Δ <i>sasA</i>	Cm	Lab collection
<i>sasA</i> -H28A	NSII-P _{kaiBC} :: <i>luc</i> . <i>sasA</i> -H28A	Cm	This study
<i>sasA</i> -N93A	NSII-P _{kaiBC} :: <i>luc</i> . <i>sasA</i> -N93A	Cm	This study
<i>sasA</i> -N93E	NSII-P _{kaiBC} :: <i>luc</i> . <i>sasA</i> -N93E	Cm	This study
<i>sasA</i> -Q94A	NSII-P _{kaiBC} :: <i>luc</i> <i>sasA</i> -Q94A	Cm	This study
<i>sasA</i> -H28A-Q94A	NSII-P _{kaiBC} :: <i>luc</i> <i>sasA</i> -H28A-Q94A	Cm	This study
<i>sasA</i> -Q97A	NSII-P _{kaiBC} :: <i>luc</i> . <i>sasA</i> -Q97A	Cm	This study
<i>sasA</i> -Q97E	NSII-P _{kaiBC} :: <i>luc</i> . <i>sasA</i> -Q97E	Cm	This study
<i>sasA</i> -Q101A	NSII-P _{kaiBC} :: <i>luc</i> <i>sasA</i> -Q101A	Cm	This study
AMC704	Δ <i>kaiC</i> / NSII-P _{kaiBC} :: <i>luc</i>	Cm	Lab collection
AMC1722	Tn5 8S15-E11 in AMC541	Cm	Boyd et al., 2013 (43)
Δ <i>rpaA</i>	<i>rpaA</i> ::Gm / NSII-P _{kaiBC} :: <i>luc</i>	Cm	This study
<i>rpaA</i> -R121Q	<i>rpaA</i> (G362->A) / NSII-P _{kaiBC} :: <i>luc</i>	Cm	This study

Table S12. Plasmids and primers used in generating cyanobacterial strains.

Plasmids	Description	Source
pSL2680	CRISPR/Cas12a plasmid; Km resistance	Addgene (#85581)
pSL2680-HA	pSL2680 + SasA H28A substitution	This study
pSL2680-NA	pSL2680 + SasA N93A substitution	This study
pSL2680-NE	pSL2680 + SasA N93E substitution	This study
pSL2680-94	pSL2680 + SasA Q94A substitution	This study
pSL2680-HA/94	pSL2680 + SasA H28A and Q94A substitutions	This study
pSL2680-97	pSL2680 + SasA Q97A substitution	This study
pSL2680-QE	pSL2680 + SasA Q97E substitution	This study
pSL2680-101	pSL2680 + SasA Q101A substitution	This study
pSL2680	RSF1010-backbone, Cas12a and CRISPR assay from <i>Francisella novicida</i> , Km ^R	Ungerer and Pakrasi, 2016 (44)
AM4523	Deletion construct containing <i>rpaA</i> ::Gm flanked by <i>S. elongatus</i> gDNA	Lab collection
pDE32	pSL2680 with gRNA targeting <i>rpaA</i> and HDR encoding <i>rpaA</i> (G362->A)	This study
Primers	Sequence (5'-3')	

Primers used for pSL2680-HA	
H28A gRNA F	AGATTGCAGCGGGTTAAAAATATT
H28A gRNA R	AGACAATATTTTTAACCCGCTGCA
H28A homology arm upstream F	TAGCTTTAATGCGGTAGTTGGTACCATGATCGACGCCTGTCTGA
H28A homology arm upstream R	TTTAACCCGCTGCACGATGGCCTGTGACAGGGGCCG
H28A homology arm downstream F	CGGCCCTGTACAGGCCATCGTGCAGCGGGTTAAA
Primers used for pSL2680-NA	
N93A gRNA F	AGATGCTAATTGATCGGTGAGGTC
N93A gRNA R	AGACGACCTCACCGATCAATTAGC
N93A homology arm upstream F	CATTTTTTTGTCTAGCTTTAATGCGGTAGTTGGTACC CTGGCGATGGACTTGCACTCA
N93A homology arm upstream R	CTGGGGCAACTGGGCGGCTAATTGATCGGT
N93A homology arm downstream F	ACCGATCAATTAGCCGCCAGTTGCCCCAG
N93A homology arm downstream R	GCCCGGATTACAGATCCTCTAGAGTCGACGGTACC TTAGCAGGGCATGGTGTAGC
Primers used for pSL2680-NE	
N93E gRNA F	AGATGCTAATTGATCGGTGAGGTC
N93E gRNA R	AGACGACCTCACCGATCAATTAGC
N93E homology arm upstream F	CATTTTTTTGTCTAGCTTTAATGCGGTAGTTGGTACC CTGGCGATGGACTTGCACTCA
N93E homology arm upstream R	CTGGGGCAACTGCTCGGCTAATTGATCGGT
N93E homology arm downstream F	ACCGATCAATTAGCCGAGCAGTTGCCCCAG
N93E homology arm downstream R	GCCCGGATTACAGATCCTCTAGAGTCGACGGTACC TTAGCAGGGCATGGTGTAGC
Primers used for pSL2680-94	
Q94A gRNA F	AGATGTTGGCTAATTGATCGGTGA
Q94AgRNA R	AGACTCACCGATCAATTAGCCAAC
Q94A homology arm upstream F	CATTTTTTTGTCTAGCTTTAATGCGGTAGTTGGTACC CTGGCGATGGACTTGCACTCA
Q94A homology arm upstream R	CCACTGGGGCAACGCGTTGGCTAATTG
Q94A homology arm downstream F	CAATTAGCCAACGCGTTGCCCCAGTGG
Q94A homology arm downstream R	GCCCGGATTACAGATCCTCTAGAGTCGACGGTACC TTAGCAGGGCATGGTGTAGC
Primers used for pSL2680 HA/94	
HA/94 gRNA F	AGATACGAAGAAAGCTCAGTGAGC
HA/94 gRNA R	AGACGCTCACTGAGCTTTCTTCGT

HA/94 homology arm upstream F	CATTTTTTTGTCTAGCTTTAATGCGGTAGTTGGTACC CTGGCGATGGACTTGCACTCA
HA/94 homology arm upstream R	GCTCACTGAGCTTTCTTCGTGTATCCGCCAAATTGT
HA94 homology arm downstream F	ACAATTTGGCGGATACACGAAGAAAGCTCAGTGAGC
HA94 homology arm downstream R	CAGATCCTCTAGAGTCGACGGTACC ATCGTGCCTGATCGAACA
Primers used for pSL2680-97	
Q97A gRNA F	AGATGGGCAACTGGTTGGCTAATT
Q97A gRNA R	AGACAATTAGCCAACCAGTTGCC
Q97A homology arm upstream F	CATTTTTTTGTCTAGCTTTAATGCGGTAGTTGGTACC CTGGCGATGGACTTGCACTCA
Q97A homology arm upstream R	CTGAACCAGCCACGCGGGCAACTGGTT
Q97A homology arm downstream F	AACCAGTTGCCCGCGTGGCTGGTTCAG
Q97A homology arm downstream R	GCCCGGATTACAGATCCTCTAGAGTCGACGGTACC TTAGCAGGGCATGGTGTAGC
Primers used for pSL2680-QE	
Q97E gRNA F	AGATTGAGTGGCATCGACCTCACC
Q97E gRNA R	AGACGGTGAGGTCGATGCCACTCA
Q97E homology arm upstream F	CATTTTTTTGTCTAGCTTTAATGCGGTAGTTGGTACC CTGGCGATGGACTTGCACTCA
Q97E homology arm upstream R	GGCTAATTGATCGGTGAGGTCGATGCCACTCAGCACTTGGC
Q97E homology arm downstream F	ACCTCACCGATCAATTAGCCAACCAGTTGCCCGAGTGGCTGG
Q97E homology arm downstream R	GCCCGGATTACAGATCCTCTAGAGTCGACGGTACC TTAGCAGGGCATGGTGTAGC
Primers used for pSL2680-101	
Q101A gRNA F	AGATAACCAGCCACTGGGGCAACT
Q101A gRNA R	AGACAGTTGCCCCAGTGGCTGGTT
Q101A homology arm upstream F	CATTTTTTTGTCTAGCTTTAATGCGGTAGTTGGTACC CTGGCGATGGACTTGCACTCA
Q101A homology arm upstream R	AAAGGCCTCTTGCGCAACCAGCCACTG
Q101A homology arm downstream F	CAGTGGCTGGTTGCGCAAGAGGCCTTT
Q101A homology arm downstream R	GCCCGGATTACAGATCCTCTAGAGTCGACGGTACC TTAGCAGGGCATGGTGTAGC
Primers used for colony PCR	
<i>sasA1_SNP_chkF</i>	CGAGTTAATGGGAGAGTCTCTGTC
<i>sasA1_SNP_chkR</i>	GGCCTAGCTCCGTGAACG
Primer used for construction of RpaA-R121Q mutant stains	

rpaA_gRNA_F	AGATGCTGAACAGCTAAAGCCTGA
rpaA_gRNA_R	AGACTCAGGCTTTAGCTGTTTCAGC
rpaA_HDR-UP_F	CATTTTTTTGTCTAGCTTTAATGCGGTAGTTGGTACCGAGTCC TGAGCTGCTACTGCC
rpaA_HDR-UP_R	GGTCAGGCTTTAGCTGTGCAGCTCGTTCCCGACCTGAT
rpaA_HDR-DWN_F	ATCAGGTCGGGAACGAGCTGCACAGCTAAAGCCTGACC
rpaA_HDR-DWN_R	GCCCGGATTACAGATCCTCTAGAGTCGACGGTACCGCCATGT CAAACCTCAATCAAGCG
rpaA_cPCR_F	GAACAGGCTGAAACGATGGC
rpaA_cPCR_R	GGATTGAGTAATTTGATGGTTGACTGC

References and Notes

1. J. C. Dunlap, J. J. Loros, P. J. DeCoursey, Eds., *Chronobiology: Biological Timekeeping* (Sinauer Associates, 2004).
2. M. A. Woelfle, Y. Ouyang, K. Phanvijhitsiri, C. H. Johnson, The adaptive value of circadian clocks: An experimental assessment in cyanobacteria. *Curr. Biol.* **14**, 1481–1486 (2004). [doi:10.1016/j.cub.2004.08.023](https://doi.org/10.1016/j.cub.2004.08.023) [Medline](#)
3. T. Kondo, C. A. Strayer, R. D. Kulkarni, W. Taylor, M. Ishiura, S. S. Golden, C. H. Johnson, Circadian rhythms in prokaryotes: Luciferase as a reporter of circadian gene expression in cyanobacteria. *Proc. Natl. Acad. Sci. U.S.A.* **90**, 5672–5676 (1993). [doi:10.1073/pnas.90.12.5672](https://doi.org/10.1073/pnas.90.12.5672) [Medline](#)
4. M. Ishiura, S. Kutsuna, S. Aoki, H. Iwasaki, C. R. Andersson, A. Tanabe, S. S. Golden, C. H. Johnson, T. Kondo, Expression of a gene cluster *kaiABC* as a circadian feedback process in cyanobacteria. *Science* **281**, 1519–1523 (1998). [doi:10.1126/science.281.5382.1519](https://doi.org/10.1126/science.281.5382.1519) [Medline](#)
5. J. Tomita, M. Nakajima, T. Kondo, H. Iwasaki, No transcription-translation feedback in circadian rhythm of KaiC phosphorylation. *Science* **307**, 251–254 (2005). [doi:10.1126/science.1102540](https://doi.org/10.1126/science.1102540) [Medline](#)
6. M. Nakajima, K. Imai, H. Ito, T. Nishiwaki, Y. Murayama, H. Iwasaki, T. Oyama, T. Kondo, Reconstitution of circadian oscillation of cyanobacterial KaiC phosphorylation in vitro. *Science* **308**, 414–415 (2005). [doi:10.1126/science.1108451](https://doi.org/10.1126/science.1108451) [Medline](#)
7. M. J. Rust, J. S. Markson, W. S. Lane, D. S. Fisher, E. K. O’Shea, Ordered phosphorylation governs oscillation of a three-protein circadian clock. *Science* **318**, 809–812 (2007). [doi:10.1126/science.1148596](https://doi.org/10.1126/science.1148596) [Medline](#)
8. T. Nishiwaki, Y. Satomi, Y. Kitayama, K. Terauchi, R. Kiyohara, T. Takao, T. Kondo, A sequential program of dual phosphorylation of KaiC as a basis for circadian rhythm in cyanobacteria. *EMBO J.* **26**, 4029–4037 (2007). [doi:10.1038/sj.emboj.7601832](https://doi.org/10.1038/sj.emboj.7601832) [Medline](#)
9. H. Iwasaki, T. Nishiwaki, Y. Kitayama, M. Nakajima, T. Kondo, KaiA-stimulated KaiC phosphorylation in circadian timing loops in cyanobacteria. *Proc. Natl. Acad. Sci. U.S.A.* **99**, 15788–15793 (2002). [doi:10.1073/pnas.222467299](https://doi.org/10.1073/pnas.222467299) [Medline](#)
10. S. B. Williams, I. Vakonakis, S. S. Golden, A. C. LiWang, Structure and function from the circadian clock protein KaiA of *Synechococcus elongatus*: A potential clock input mechanism. *Proc. Natl. Acad. Sci. U.S.A.* **99**, 15357–15362 (2002). [doi:10.1073/pnas.232517099](https://doi.org/10.1073/pnas.232517099) [Medline](#)
11. Y. Kitayama, H. Iwasaki, T. Nishiwaki, T. Kondo, KaiB functions as an attenuator of KaiC phosphorylation in the cyanobacterial circadian clock system. *EMBO J.* **22**, 2127–2134 (2003). [doi:10.1093/emboj/cdg212](https://doi.org/10.1093/emboj/cdg212) [Medline](#)
12. Y. Xu, T. Mori, C. H. Johnson, Cyanobacterial circadian clockwork: Roles of KaiA, KaiB and the *kaiBC* promoter in regulating KaiC. *EMBO J.* **22**, 2117–2126 (2003). [doi:10.1093/emboj/cdg168](https://doi.org/10.1093/emboj/cdg168) [Medline](#)

13. Y.-G. Chang, R. Tseng, N.-W. Kuo, A. LiWang, Rhythmic ring-ring stacking drives the circadian oscillator clockwise. *Proc. Natl. Acad. Sci. U.S.A.* **109**, 16847–16851 (2012). [doi:10.1073/pnas.1211508109](https://doi.org/10.1073/pnas.1211508109) [Medline](#)
14. Y.-G. Chang, N.-W. Kuo, R. Tseng, A. LiWang, Flexibility of the C-terminal, or CII, ring of KaiC governs the rhythm of the circadian clock of cyanobacteria. *Proc. Natl. Acad. Sci. U.S.A.* **108**, 14431–14436 (2011). [doi:10.1073/pnas.1104221108](https://doi.org/10.1073/pnas.1104221108) [Medline](#)
15. J. Abe, T. B. Hiyama, A. Mukaiyama, S. Son, T. Mori, S. Saito, M. Osako, J. Wolanin, E. Yamashita, T. Kondo, S. Akiyama, Atomic-scale origins of slowness in the cyanobacterial circadian clock. *Science* **349**, 312–316 (2015). [doi:10.1126/science.1261040](https://doi.org/10.1126/science.1261040) [Medline](#)
16. H. Iwasaki, S. B. Williams, Y. Kitayama, M. Ishiura, S. S. Golden, T. Kondo, A KaiC-interacting sensory histidine kinase, SasA, necessary to sustain robust circadian oscillation in cyanobacteria. *Cell* **101**, 223–233 (2000). [doi:10.1016/S0092-8674\(00\)80832-6](https://doi.org/10.1016/S0092-8674(00)80832-6) [Medline](#)
17. O. Schmitz, M. Katayama, S. B. Williams, T. Kondo, S. S. Golden, CikA, a bacteriophytochrome that resets the cyanobacterial circadian clock. *Science* **289**, 765–768 (2000). [doi:10.1126/science.289.5480.765](https://doi.org/10.1126/science.289.5480.765) [Medline](#)
18. N. B. Ivleva, T. Gao, A. C. LiWang, S. S. Golden, Quinone sensing by the circadian input kinase of the cyanobacterial circadian clock. *Proc. Natl. Acad. Sci. U.S.A.* **103**, 17468–17473 (2006). [doi:10.1073/pnas.0606639103](https://doi.org/10.1073/pnas.0606639103) [Medline](#)
19. N. Takai, M. Nakajima, T. Oyama, R. Kito, C. Sugita, M. Sugita, T. Kondo, H. Iwasaki, A KaiC-associating SasA-RpaA two-component regulatory system as a major circadian timing mediator in cyanobacteria. *Proc. Natl. Acad. Sci. U.S.A.* **103**, 12109–12114 (2006). [doi:10.1073/pnas.0602955103](https://doi.org/10.1073/pnas.0602955103) [Medline](#)
20. J. S. Markson, J. R. Piechura, A. M. Puszynska, E. K. O’Shea, Circadian control of global gene expression by the cyanobacterial master regulator RpaA. *Cell* **155**, 1396–1408 (2013). [doi:10.1016/j.cell.2013.11.005](https://doi.org/10.1016/j.cell.2013.11.005) [Medline](#)
21. A. Gutu, E. K. O’Shea, Two antagonistic clock-regulated histidine kinases time the activation of circadian gene expression. *Mol. Cell* **50**, 288–294 (2013). [doi:10.1016/j.molcel.2013.02.022](https://doi.org/10.1016/j.molcel.2013.02.022) [Medline](#)
22. K. Ito-Miwa, Y. Furuike, S. Akiyama, T. Kondo, Tuning the circadian period of cyanobacteria up to 6.6 days by the single amino acid substitutions in KaiC. *Proc. Natl. Acad. Sci. U.S.A.* **117**, 20926–20931 (2020). [doi:10.1073/pnas.2005496117](https://doi.org/10.1073/pnas.2005496117) [Medline](#)
23. E. Leypunskiy, J. Lin, H. Yoo, U. Lee, A. R. Dinner, M. J. Rust, The cyanobacterial circadian clock follows midday in vivo and in vitro. *eLife* **6**, e23539 (2017). [doi:10.7554/eLife.23539](https://doi.org/10.7554/eLife.23539) [Medline](#)
24. G. K. Chow, A. G. Chavan, J. C. Heisler, Y.-G. Chang, A. LiWang, R. D. Britt, Monitoring protein–protein interactions in the cyanobacterial circadian clock in real time via electron paramagnetic resonance spectroscopy. *Biochemistry* **59**, 2387–2400 (2020). [doi:10.1021/acs.biochem.0c00279](https://doi.org/10.1021/acs.biochem.0c00279) [Medline](#)

25. J. Heisler, A. Chavan, Y.-G. Chang, A. LiWang, Real-time in vitro fluorescence anisotropy of the cyanobacterial circadian clock. *Methods Protoc.* **2**, 42 (2019).
[doi:10.3390/mps2020042](https://doi.org/10.3390/mps2020042) [Medline](#)
26. C. S. Theile, M. D. Witte, A. E. M. Blom, L. Kundrat, H. L. Ploegh, C. P. Guimaraes, Site-specific N-terminal labeling of proteins using sortase-mediated reactions. *Nat. Protoc.* **8**, 1800–1807 (2013). [doi:10.1038/nprot.2013.102](https://doi.org/10.1038/nprot.2013.102) [Medline](#)
27. C. P. Guimaraes, M. D. Witte, C. S. Theile, G. Bozkurt, L. Kundrat, A. E. M. Blom, H. L. Ploegh, Site-specific C-terminal and internal loop labeling of proteins using sortase-mediated reactions. *Nat. Protoc.* **8**, 1787–1799 (2013). [doi:10.1038/nprot.2013.101](https://doi.org/10.1038/nprot.2013.101) [Medline](#)
28. B. Guo, P. S. Gurel, R. Shu, H. N. Higgs, M. Pellegrini, D. F. Mierke, Monitoring ATP hydrolysis and ATPase inhibitor screening using ¹H NMR. *Chem. Commun.* **50**, 12037–12039 (2014). [doi:10.1039/C4CC04399E](https://doi.org/10.1039/C4CC04399E) [Medline](#)
29. K. Terauchi, Y. Kitayama, T. Nishiwaki, K. Miwa, Y. Murayama, T. Oyama, T. Kondo, ATPase activity of KaiC determines the basic timing for circadian clock of cyanobacteria. *Proc. Natl. Acad. Sci. U.S.A.* **104**, 16377–16381 (2007).
[doi:10.1073/pnas.0706292104](https://doi.org/10.1073/pnas.0706292104) [Medline](#)
30. R. M. Smith, S. B. Williams, Circadian rhythms in gene transcription imparted by chromosome compaction in the cyanobacterium *Synechococcus elongatus*. *Proc. Natl. Acad. Sci. U.S.A.* **103**, 8564–8569 (2006). [doi:10.1073/pnas.0508696103](https://doi.org/10.1073/pnas.0508696103) [Medline](#)
31. S. E. Cohen, S. S. Golden, Circadian rhythms in cyanobacteria. *Microbiol. Mol. Biol. Rev.* **79**, 373–385 (2015). [doi:10.1128/MMBR.00036-15](https://doi.org/10.1128/MMBR.00036-15) [Medline](#)
32. H. Kageyama, T. Kondo, H. Iwasaki, Circadian formation of clock protein complexes by KaiA, KaiB, KaiC, and SasA in cyanobacteria. *J. Biol. Chem.* **278**, 2388–2395 (2003).
[doi:10.1074/jbc.M208899200](https://doi.org/10.1074/jbc.M208899200) [Medline](#)
33. R. Tseng, Y.-G. Chang, I. Bravo, R. Latham, A. Chaudhary, N.-W. Kuo, A. Liwang, Cooperative KaiA-KaiB-KaiC interactions affect KaiB/SasA competition in the circadian clock of cyanobacteria. *J. Mol. Biol.* **426**, 389–402 (2014).
[doi:10.1016/j.jmb.2013.09.040](https://doi.org/10.1016/j.jmb.2013.09.040) [Medline](#)
34. P. B. Straughn, L. R. Vass, C. Yuan, E. N. Kennedy, C. A. Foster, R. B. Bourret, Modulation of response regulator CheY reaction kinetics by two variable residues that affect conformation. *J. Bacteriol.* **202**, e00089-20 (2020). [doi:10.1128/JB.00089-20](https://doi.org/10.1128/JB.00089-20) [Medline](#)
35. A. H. West, A. M. Stock, Histidine kinases and response regulator proteins in two-component signaling systems. *Trends Biochem. Sci.* **26**, 369–376 (2001).
[doi:10.1016/S0968-0004\(01\)01852-7](https://doi.org/10.1016/S0968-0004(01)01852-7) [Medline](#)
36. R. Tseng, N. F. Goularte, A. Chavan, J. Luu, S. E. Cohen, Y.-G. Chang, J. Heisler, S. Li, A. K. Michael, S. Tripathi, S. S. Golden, A. LiWang, C. L. Partch, Structural basis of the day-night transition in a bacterial circadian clock. *Science* **355**, 1174–1180 (2017).
[doi:10.1126/science.aag2516](https://doi.org/10.1126/science.aag2516) [Medline](#)
37. Y.-G. Chang, S. E. Cohen, C. Phong, W. K. Myers, Y.-I. Kim, R. Tseng, J. Lin, L. Zhang, J. S. Boyd, Y. Lee, S. Kang, D. Lee, S. Li, R. D. Britt, M. J. Rust, S. S. Golden, A. LiWang,

- A protein fold switch joins the circadian oscillator to clock output in cyanobacteria. *Science* **349**, 324–328 (2015). [doi:10.1126/science.1260031](https://doi.org/10.1126/science.1260031) [Medline](#)
38. N. B. Ivleva, M. R. Bramlett, P. A. Lindahl, S. S. Golden, LdpA: A component of the circadian clock senses redox state of the cell. *EMBO J.* **24**, 1202–1210 (2005). [doi:10.1038/sj.emboj.7600606](https://doi.org/10.1038/sj.emboj.7600606) [Medline](#)
 39. Y. Taniguchi, N. Takai, M. Katayama, T. Kondo, T. Oyama, Three major output pathways from the KaiABC-based oscillator cooperate to generate robust circadian *kaiBC* expression in cyanobacteria. *Proc. Natl. Acad. Sci. U.S.A.* **107**, 3263–3268 (2010). [doi:10.1073/pnas.0909924107](https://doi.org/10.1073/pnas.0909924107) [Medline](#)
 40. M. J. Rust, S. S. Golden, E. K. O’Shea, Light-driven changes in energy metabolism directly entrain the cyanobacterial circadian oscillator. *Science* **331**, 220–223 (2011). [doi:10.1126/science.1197243](https://doi.org/10.1126/science.1197243) [Medline](#)
 41. Y.-I. Kim, D. J. Vinyard, G. M. Ananyev, G. C. Dismukes, S. S. Golden, Oxidized quinones signal onset of darkness directly to the cyanobacterial circadian oscillator. *Proc. Natl. Acad. Sci. U.S.A.* **109**, 17765–17769 (2012). [doi:10.1073/pnas.1216401109](https://doi.org/10.1073/pnas.1216401109) [Medline](#)
 42. M. L. Paddock, J. S. Boyd, D. M. Adin, S. S. Golden, Active output state of the *Synechococcus* Kai circadian oscillator. *Proc. Natl. Acad. Sci. U.S.A.* **110**, E3849–E3857 (2013). [doi:10.1073/pnas.1315170110](https://doi.org/10.1073/pnas.1315170110) [Medline](#)
 43. J. S. Boyd, J. R. Bordowitz, A. C. Bree, S. S. Golden, An allele of the *crm* gene blocks cyanobacterial circadian rhythms. *Proc. Natl. Acad. Sci. U.S.A.* **110**, 13950–13955 (2013). [doi:10.1073/pnas.1312793110](https://doi.org/10.1073/pnas.1312793110) [Medline](#)
 44. J. Ungerer, H. B. Pakrasi, Cpf1 is a versatile tool for CRISPR genome editing across diverse species of cyanobacteria. *Sci. Rep.* **6**, 39681 (2016). [doi:10.1038/srep39681](https://doi.org/10.1038/srep39681) [Medline](#)
 45. M. Nakajima, H. Ito, T. Kondo, *In vitro* regulation of circadian phosphorylation rhythm of cyanobacterial clock protein KaiC by KaiA and KaiB. *FEBS Lett.* **584**, 898–902 (2010). [doi:10.1016/j.febslet.2010.01.016](https://doi.org/10.1016/j.febslet.2010.01.016) [Medline](#)
 46. J. Chew, E. Leypunskiy, J. Lin, A. Murugan, M. J. Rust, High protein copy number is required to suppress stochasticity in the cyanobacterial circadian clock. *Nat. Commun.* **9**, 3004 (2018). [doi:10.1038/s41467-018-05109-4](https://doi.org/10.1038/s41467-018-05109-4) [Medline](#)
 47. J. Lin, J. Chew, U. Chockanathan, M. J. Rust, Mixtures of opposing phosphorylations within hexamers precisely time feedback in the cyanobacterial circadian clock. *Proc. Natl. Acad. Sci. U.S.A.* **111**, E3937–E3945 (2014). [doi:10.1073/pnas.1408692111](https://doi.org/10.1073/pnas.1408692111) [Medline](#)
 48. M. Kaur, A. Ng, P. Kim, C. Diekman, Y.-I. Kim, CikA modulates the effect of KaiA on the period of the circadian oscillation in KaiC phosphorylation. *J. Biol. Rhythms* **34**, 218–223 (2019). [doi:10.1177/0748730419828068](https://doi.org/10.1177/0748730419828068) [Medline](#)
 49. R. Murakami, R. Mutoh, R. Iwase, Y. Furukawa, K. Imada, K. Onai, M. Morishita, S. Yasui, K. Ishii, J. O. Valencia Swain, T. Uzumaki, K. Namba, M. Ishiura, The roles of the dimeric and tetrameric structures of the clock protein KaiB in the generation of circadian oscillations in cyanobacteria. *J. Biol. Chem.* **287**, 29506–29515 (2012). [doi:10.1074/jbc.M112.349092](https://doi.org/10.1074/jbc.M112.349092) [Medline](#)

50. J. Valencia S., K. Bitou, K. Ishii, R. Murakami, M. Morishita, K. Onai, Y. Furukawa, K. Imada, K. Namba, M. Ishiura, Phase-dependent generation and transmission of time information by the KaiABC circadian clock oscillator through SasA-KaiC interaction in cyanobacteria. *Genes Cells* **17**, 398–419 (2012). [doi:10.1111/j.1365-2443.2012.01597.x](https://doi.org/10.1111/j.1365-2443.2012.01597.x) [Medline](#)
51. J. Snijder, J. M. Schuller, A. Wiegard, P. Lössl, N. Schmelling, I. M. Axmann, J. M. Plitzko, F. Förster, A. J. R. Heck, Structures of the cyanobacterial circadian oscillator frozen in a fully assembled state. *Science* **355**, 1181–1184 (2017). [doi:10.1126/science.aag3218](https://doi.org/10.1126/science.aag3218) [Medline](#)
52. R. Murakami, Y. Yunoki, K. Ishii, K. Terauchi, S. Uchiyama, H. Yagi, K. Kato, Cooperative binding of KaiB to the KaiC hexamer ensures accurate circadian clock oscillation in cyanobacteria. *Int. J. Mol. Sci.* **20**, 4550 (2019). [doi:10.3390/ijms20184550](https://doi.org/10.3390/ijms20184550) [Medline](#)
53. J. Snijder, R. J. Burnley, A. Wiegard, A. S. J. Melquiond, A. M. J. J. Bonvin, I. M. Axmann, A. J. R. Heck, Insight into cyanobacterial circadian timing from structural details of the KaiB-KaiC interaction. *Proc. Natl. Acad. Sci. U.S.A.* **111**, 1379–1384 (2014). [doi:10.1073/pnas.1314326111](https://doi.org/10.1073/pnas.1314326111) [Medline](#)
54. R. G. Garces, N. Wu, W. Gillon, E. F. Pai, Anabaena circadian clock proteins KaiA and KaiB reveal a potential common binding site to their partner KaiC. *EMBO J.* **23**, 1688–1698 (2004). [doi:10.1038/sj.emboj.7600190](https://doi.org/10.1038/sj.emboj.7600190) [Medline](#)
55. Y. Xu, T. Mori, C. H. Johnson, Circadian clock-protein expression in cyanobacteria: Rhythms and phase setting. *EMBO J.* **19**, 3349–3357 (2000). [doi:10.1093/emboj/19.13.3349](https://doi.org/10.1093/emboj/19.13.3349) [Medline](#)
56. C. K. Holtman, Y. Chen, P. Sandoval, A. Gonzales, M. S. Nalty, T. L. Thomas, P. Youderian, S. S. Golden, High-throughput functional analysis of the *Synechococcus elongatus* PCC 7942 genome. *DNA Res.* **12**, 103–115 (2005). [doi:10.1093/dnares/12.2.103](https://doi.org/10.1093/dnares/12.2.103) [Medline](#)
57. K. Imai, Y. Kitayama, T. Kondo, Elucidation of the role of Clp protease components in circadian rhythm by genetic deletion and overexpression in cyanobacteria. *J. Bacteriol.* **195**, 4517–4526 (2013). [doi:10.1128/JB.00300-13](https://doi.org/10.1128/JB.00300-13) [Medline](#)
58. H. Liu, J. H. Naismith, An efficient one-step site-directed deletion, insertion, single and multiple-site plasmid mutagenesis protocol. *BMC Biotechnol.* **8**, 91 (2008). [doi:10.1186/1472-6750-8-91](https://doi.org/10.1186/1472-6750-8-91) [Medline](#)
59. C. A. Schneider, W. S. Rasband, K. W. Eliceiri, NIH Image to ImageJ: 25 years of image analysis. *Nat. Methods* **9**, 671–675 (2012). [doi:10.1038/nmeth.2089](https://doi.org/10.1038/nmeth.2089) [Medline](#)
60. A. Moore, T. Zielinski, A. J. Millar, Online period estimation and determination of rhythmicity in circadian data, using the BioDare data infrastructure. *Methods Mol. Biol.* **1158**, 13–44 (2014). [doi:10.1007/978-1-4939-0700-7_2](https://doi.org/10.1007/978-1-4939-0700-7_2) [Medline](#)
61. T. Zielinski, A. M. Moore, E. Troup, K. J. Halliday, A. J. Millar, Strengths and limitations of period estimation methods for circadian data. *PLOS ONE* **9**, e96462 (2014). [doi:10.1371/journal.pone.0096462](https://doi.org/10.1371/journal.pone.0096462) [Medline](#)

62. S. R. Mackey, J. L. Ditty, E. M. Clerico, S. S. Golden, Detection of rhythmic bioluminescence from luciferase reporters in cyanobacteria. *Methods Mol. Biol.* **362**, 115–129 (2007). [doi:10.1007/978-1-59745-257-1_8](https://doi.org/10.1007/978-1-59745-257-1_8) [Medline](#)
63. A. Taton, F. Unglaub, N. E. Wright, W. Y. Zeng, J. Paz-Yepes, B. Brahamsha, B. Palenik, T. C. Peterson, F. Haerizadeh, S. S. Golden, J. W. Golden, Broad-host-range vector system for synthetic biology and biotechnology in cyanobacteria. *Nucleic Acids Res.* **42**, e136 (2014). [doi:10.1093/nar/gku673](https://doi.org/10.1093/nar/gku673) [Medline](#)
64. E. M. Clerico, J. L. Ditty, S. S. Golden, Specialized techniques for site-directed mutagenesis in cyanobacteria. *Methods Mol. Biol.* **362**, 155–171 (2007). [doi:10.1007/978-1-59745-257-1_11](https://doi.org/10.1007/978-1-59745-257-1_11) [Medline](#)
65. J. Elhai, A. Vepritskiy, A. M. Muro-Pastor, E. Flores, C. P. Wolk, Reduction of conjugal transfer efficiency by three restriction activities of *Anabaena* sp. strain PCC 7120. *J. Bacteriol.* **179**, 1998–2005 (1997). [doi:10.1128/jb.179.6.1998-2005.1997](https://doi.org/10.1128/jb.179.6.1998-2005.1997) [Medline](#)
66. J. Elhai, C. P. Wolk, “Conjugal transfer of DNA to cyanobacteria” in *Cyanobacteria*, vol. 167 of *Methods in Enzymology*, L. Packer, A. N. Glazer, Eds. (Elsevier, 1988), pp. 747–754.
67. S. S. Golden, L. A. Sherman, Optimal conditions for genetic transformation of the cyanobacterium *Anacystis nidulans* R2. *J. Bacteriol.* **158**, 36–42 (1984). [doi:10.1128/jb.158.1.36-42.1984](https://doi.org/10.1128/jb.158.1.36-42.1984) [Medline](#)
68. A. Taton, E. Lis, D. M. Adin, G. Dong, S. Cookson, S. A. Kay, S. S. Golden, J. W. Golden, Gene transfer in *Leptolyngbya* sp. strain BL0902, a cyanobacterium suitable for production of biomass and bioproducts. *PLOS ONE* **7**, e30901 (2012). [doi:10.1371/journal.pone.0030901](https://doi.org/10.1371/journal.pone.0030901) [Medline](#)
- <jrn>69. N. B. Ivleva, S. S. Golden, Protein extraction, fractionation, and purification from cyanobacteria. *Methods Mol. Biol.* **362**, 365–373 (2007). [doi:10.1007/978-1-59745-257-1_26](https://doi.org/10.1007/978-1-59745-257-1_26) [Medline](#)</jrn>
70. D. G. Welkie, B. E. Rubin, Y.-G. Chang, S. Diamond, S. A. Rifkin, A. LiWang, S. S. Golden, Genome-wide fitness assessment during diurnal growth reveals an expanded role of the cyanobacterial circadian clock protein KaiA. *Proc. Natl. Acad. Sci. U.S.A.* **115**, E7174–E7183 (2018). [doi:10.1073/pnas.1802940115](https://doi.org/10.1073/pnas.1802940115) [Medline](#)
71. T. G. G. Battye, L. Kontogiannis, O. Johnson, H. R. Powell, A. G. W. Leslie, *iMOSFLM*: A new graphical interface for diffraction-image processing with *MOSFLM*. *Acta Crystallogr. D* **67**, 271–281 (2011). [doi:10.1107/S0907444910048675](https://doi.org/10.1107/S0907444910048675) [Medline](#)
72. P. R. Evans, G. N. Murshudov, How good are my data and what is the resolution? *Acta Crystallogr. D* **69**, 1204–1214 (2013). [doi:10.1107/S0907444913000061](https://doi.org/10.1107/S0907444913000061) [Medline](#)
73. A. J. McCoy, R. W. Grosse-Kunstleve, P. D. Adams, M. D. Winn, L. C. Storoni, R. J. Read, *Phaser* crystallographic software. *J. Appl. Crystallogr.* **40**, 658–674 (2007). [doi:10.1107/S0021889807021206](https://doi.org/10.1107/S0021889807021206) [Medline](#)
74. D. Liebschner, P. V. Afonine, M. L. Baker, G. Bunkóczi, V. B. Chen, T. I. Croll, B. Hintze, L.-W. Hung, S. Jain, A. J. McCoy, N. W. Moriarty, R. D. Oeffner, B. K. Poon, M. G. Prisant, R. J. Read, J. S. Richardson, D. C. Richardson, M. D. Sammito, O. V. Sobolev,

- D. H. Stockwell, T. C. Terwilliger, A. G. Urzhumtsev, L. L. Videau, C. J. Williams, P. D. Adams, Macromolecular structure determination using X-rays, neutrons and electrons: Recent developments in *Phenix*. *Acta Crystallogr. D* **75**, 861–877 (2019). [doi:10.1107/S2059798319011471](https://doi.org/10.1107/S2059798319011471) [Medline](#)
75. P. Emsley, B. Lohkamp, W. G. Scott, K. Cowtan, Features and development of *Coot*. *Acta Crystallogr. D* **66**, 486–501 (2010). [doi:10.1107/S0907444910007493](https://doi.org/10.1107/S0907444910007493) [Medline](#)
76. E. F. Pettersen, T. D. Goddard, C. C. Huang, G. S. Couch, D. M. Greenblatt, E. C. Meng, T. E. Ferrin, UCSF Chimera—A visualization system for exploratory research and analysis. *J. Comput. Chem.* **25**, 1605–1612 (2004). [doi:10.1002/jcc.20084](https://doi.org/10.1002/jcc.20084) [Medline](#)
77. M. F. Sanner, A. J. Olson, J. C. Spehner, Reduced surface: An efficient way to compute molecular surfaces. *Biopolymers* **38**, 305–320 (1996). [doi:10.1002/\(SICI\)1097-0282\(199603\)38:3<305:AID-BIP4>3.0.CO;2-Y](https://doi.org/10.1002/(SICI)1097-0282(199603)38:3<305:AID-BIP4>3.0.CO;2-Y) [Medline](#)
78. E. F. Pettersen, T. D. Goddard, C. C. Huang, E. C. Meng, G. S. Couch, T. I. Croll, J. H. Morris, T. E. Ferrin, UCSF ChimeraX: Structure visualization for researchers, educators, and developers. *Protein Sci.* **30**, 70–82 (2021). [doi:10.1002/pro.3943](https://doi.org/10.1002/pro.3943) [Medline](#)
79. C. R. Bagshaw, *Biomolecular Kinetics: A Step-by-Step Guide* (CRC Press, 2017).
80. P. Kuzmič, Program DYNAFIT for the analysis of enzyme kinetic data: Application to HIV proteinase. *Anal. Biochem.* **237**, 260–273 (1996). [doi:10.1006/abio.1996.0238](https://doi.org/10.1006/abio.1996.0238) [Medline](#)
81. J. A. Goodrich, J. F. Kugel, *Binding and Kinetics for Molecular Biologists* (Cold Spring Harbor Laboratory Press, 2007).
82. H. Kageyama, T. Nishiwaki, M. Nakajima, H. Iwasaki, T. Oyama, T. Kondo, Cyanobacterial circadian pacemaker: Kai protein complex dynamics in the KaiC phosphorylation cycle in vitro. *Mol. Cell* **23**, 161–171 (2006). [doi:10.1016/j.molcel.2006.05.039](https://doi.org/10.1016/j.molcel.2006.05.039) [Medline](#)